EFFECT OF EARTHQUAKE VIBRATION ON SHEAR

STRENGTH OF SANDSTONE FRACTURES

Khanaphot Boonyord

A Thesis Submitted in Partial Fulfillment of the Requirements for the

Degree of Master of Engineering in Geotechnology

Suranaree University of Technology

Academic Year 2017

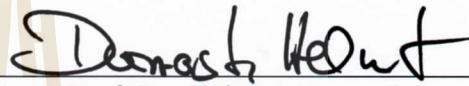# ผลกระทบของคลื่นสั่นสะเทือนแผ่นดินไหวต่อค่ากำลังรับแรงเฉือนในรอยแตกหินทราย

นายคณพศ บุญยอด

วิทยานิพนธ์นี้เป็นส่วนหนึ่งของการศึกษาตามหลักสูตรปริญญาวิศวกรรมศาสตรมหาบัณฑิต
สาขาวิชาเทคโนโลยีธรณี
มหาวิทยาลัยเทคโนโลยีสุรนารี
ปีการศึกษา 2560

EFFECT OF EARTHQUAKE VIBRATION ON SHEAR

STRENGTH OF SANDSTONE FRACTURES

Suranaree University of Technology has approved this thesis submitted in partial fulfillment of the requirements for a Master's Degree.
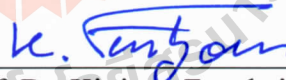
Thesis Examining Committee

_____

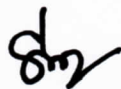(Asst. Prof. Dr. Helmut Durrast)

Chairperson

_____

(Asst. Prof. Dr. Prachya Tepnarong)
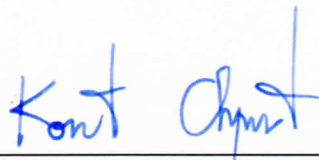
Member (Thesis Advisor)

_____

(Prof. Dr. Kittitep Fuenkajorn)

Member

_____

(Prof. Dr. Santi Maensiri)

Vice Rector for Academic Affairs

and Internationalization

_____

(Assoc. Prof. Flt. Lt. Dr. Kontorn Chamniprasart)

Dean of Institute of Engineering

คณพศ บุญยอด : ผลกระทบของคลื่นสั่นสะเทือนแผ่นดิวไหวต่อค่ากำลังรับแรงเฉือนใน
รอยแตกหินทราย (EFFECT OF EARTHQUAKE VIBRATION ON SHEAR STRENGTH
OF SANDSTONE FRACTURE) อาจารย์ที่ปรึกษา : ผู้ช่วยศาสตราจารย์
ดร. ปรัชญา เทพณรงค์, 81 หน้า

เครื่องทดสอบแรงเฉือนแบบสองรอยแตกที่ติดตั้งบนโต๊ะเขย่าถูกพัฒนาขึ้นเพื่อศึกษา
ผลกระทบของคลื่นสั่นสะเทือนจากแผ่นดินไหวต่อค่ากำลังรับแรงเฉือนของรอยแตกในหินทราย
ชุดพระวิหารขนาด 100×100×225 ลูกบาศก์มิลลิเมตร รอยแตกแบบขนานในตัวอย่างหินได้ถูกสร้าง
ขึ้นภายในห้องปฏิบัติการด้วยวิธีการให้แรงดึงและการใช้เลื่อยตัด พฤติกรรมการเฉือนของรอยแตก
ถูกตรวจสอบภายใต้แรงตั้งฉากคงที่ในสภาวะสถิตและพลวัต โดยควบคุมความเค้นตั้งฉากคงให้ผัน
แปรจาก 0.05 จนถึง 4 เมกะปาสคาล ด้วยอัตราการเฉือน 0.01 เมกะปาสคาลต่อวินาที ค่าความเร่ง
พื้นดินแนวราบของแรงสั่นสะเทือนผันแปรจาก 0.2 ถึง 0.8 เท่าของค่าแรงโน้มถ่วง (g) ผลการ
ทดสอบระบุว่าค่ากำลังรับแรงเฉือนบนรอยแตกผิวเรียบมีค่าลดลงเมื่อความเร่งแนวราบมีค่าสูงขึ้น
ในขณะที่กำลังรับแรงเฉือนบนรอยแตกผิวขรุขระมีความผันผวนเล็กน้อย ผลการทดสอบแสดงให้
เห็นอย่างเด่นชัดว่าแรงสั่นสะเทือนแผ่นดินไหวในหนึ่งมิติมีผลกระทบเพียงเล็กน้อยต่อค่ากำลังรับ
แรงเฉือนในทุกการทดสอบ โดยเฉพาะอย่างยิ่งภายใต้ค่าความเค้นตั้งฉากที่มีค่าสูง สมการทาง
คณิตศาสตร์บนพื้นฐานของเกณฑ์คูลอมบ์ที่พิจารณาถึงผลกระทบจากค่าความเร่งของ
แรงสั่นสะเทือนในแนวราบจึงได้ถูกเสนอเพื่อใช้ในการประเมินค่ากำลังรับแรงเฉือน ผลการศึกษา
สามารถใช้วิเคราะห์และออกแบบงานโครงสร้างทางวิศวกรรมในมวลหินที่มีรอยแตกภายใต้สภาวะ
การสั่นสะเทือนของแผ่นดินไหวและงานระเบิด

สาขาวิชา เทคโนโลยีธรณี	ลายมือชื่อนักศึกษา_____
ปีการศึกษา 2560	ลายมือชื่ออาจารย์ที่ปรึกษา P. Tepnarong

KHANAPHOT BOONYORD : EFFECT OF EARTHQUAKE VIBRATION ON SHEAR STRENGTH OF SANDSTONE FRACTURE. THESIS ADVISOR : ASST. PROF. PRACHYA TEPNARONG, Ph.D., 81 PP.

DOUBLE SHEAR/GROUND ACCELERATION/SHAKING TABLE/SANDSTONE

A double fracture shear test platform installed on a shaking table is developed to determine the effect of earthquake vibration on shear strength of fractures in Phra Wihan sandstone with nominal size of $100 \times 100 \times 225$ mm^3. The parallel fractures of specimen are artificially made in the laboratory by tension inducing and smooth saw-cut methods. Shear behavior of rock joints was investigated under constant normal load, static and dynamic conditions. The normal stresses are maintained constant from 0.05 to 4.0 MPa with constant shear rate of 0.01 MPa/s. The ground acceleration values of vibration are varied from 0.2 g to 0.8 g. The results indicate that the shear strengths on smooth surface decrease with increasing horizontal acceleration, whereas the shear strength on rough surface slightly fluctuates. The results clearly show that the earthquake vibration in one-dimensional very slightly affect to the shear strength for all testing, especially under high normal loads. The mathematical equations based on Coulomb criteria that explicitly incorporates the effects of horizontal ground acceleration is proposed to estimate the shear strengths. The findings can be used for the analysis and design of engineering structures in fractured rock mass under earthquake conditions and blasting activities.

School of Geotechnology

Academic Year 2017

Student's Signature_____

Advisor's Signature P. Tepnarong

ACKNOWLEDGMENTS

I would like to express my sincere thanks to Asst. Prof. Dr. Prachya Tepnarong for his valuable guidance and efficient supervision. I appreciate his strong support, encouragement, suggestions and comments during the research period. I also would like to express my gratitude to Prof. Dr. Kittitep Fuenkajorn and Asst. Prof. Dr. Helmut Durrast for their constructive advice, valuable suggestions and comments on my research works as thesis committee members. Grateful thanks are given to all staffs of Geomechanics Research Unit, Institute of Engineering who supported my work.

Finally, I would like to thank beloved parents for their love, support and encouragement.

Khanaphot Boonyord

TABLE OF CONTENTS

Page

TABLE OF CONTENTS (Continued)

TABLE OF CONTENTS (Continued)

LIST OF TABLES

LIST OF TABLES (Continued)

Table   **Page**

LIST OF FIGURES

LIST OF FIGURES (Continued)

LIST OF FIGURES (Continued)

LIST OF FIGURES (Continued)

SYMBOLS AND ABBREVIATIONS

α_{AB} = Angular acceleration

α = Empirical constant for equation (6.2)

β = Empirical constant for equation (6.2)

γ = Empirical constant for equation (6.3)

δ = Apparent friction angle of the saw-cut fractures on horizontal acceleration condition

ζ = Apparent cohesion of the saw-cut fractures on horizontal acceleration condition

η = Empirical constant for equation (6.3)

θ = Angle between AO and OB

α_R = Empirical constant for equation (6.6)

β_R = Empirical constant for equation (6.6)

γ_R = Empirical constant for equation (6.7)

δ_R = Apparent friction angle of the tension-induced fractures on horizontal acceleration condition

SYMBOLS AND ABBREVIATIONS (Continued)

ζ_R =   Apparent cohesion of the tension-induced fractures on horizontal acceleration condition

η_R =   Empirical constant for equation (6.7)

σ_c =   Compressive strengths

σ_j =   Joint wall compressive strength

σ_n =   Normal Stress

τ =   Shear Strength

τ_d =   Shear strength of driving

τ_r =   Shear strength of resisting

ϕ =   Friction Angle

ϕ_b =   Basic friction angle

ω =   Angular Velocity

A =   Linear acceleration

a_h =   Horizontal pseudo-static accelerations

a_v =   Vertical pseudo-static accelerations

SYMBOLS AND ABBREVIATIONS (Continued)

f_h =   Horizontal inertia force

FOS   =   Factor of safety

f_v =   Vertical inertia force

G   =   Ground acceleration

JRC   =   Joint roughness coefficient

k_h =   Horizontal pseudo-static coefficients

k_v =   Vertical pseudo-static coefficients

N_{Driven} =   Cycle of gear on the driven gear

n_{Driven} =   Number of teeth on the driven gear

N_{Driver} =   Cycle of gear on the driver gear

n_{Driver} =   Number of teeth on the driver gear

R   =   Radius of wheel

rpm   =   revolutions per Minute of a motor

T   =   Duration of flywheel rotation

W   =   Potential sliding mass

Y   =   Length of crack arm

CHAPTER I

INTRODUCTION

1.1 background and Rationale

Joint shear strength is one of the key properties used in the stability analysis and design of engineering structures in rock mass, e.g. slopes, tunnels and foundations. The conventional method currently used to determine the joint shear strength is the direct shear testing (e.g. ASTM D5607-08). Most of the standard testing on the mechanical properties of rock joints have been focused on determining the peak shear strength and the stress-displacement relations under unidirectional shear loading. Direct shear testing due to ground acceleration can however affect the shear strength. Kamonpet et al. (2012) performed a direct shear test to study the behavior of rock fractures under cyclic shear loading. It can be seen that the direct shear testing has been kept as simple as possible yet is adequately sensitive to most testing situations. There are several inherent advantages including rapid set up and testing time, small size and simple constant normal load system (Hencher and Richards, 1989).

The joint properties such as roughness, asperities strength, separation, gouge and even the spatial distributions make the behavior of jointed rock masses more complicated (Lee et al., 2001). In addition, the shear displacements due to earthquake loadings can also affect the shear strength. Several researchers suggest that the earthquake can affect the shear strength properties. Jafari et al (2002) concluded that small repetitive earthquakes cannot make a considerable movement, but because of

their repetitive nature, they may affect the shear resistance of rock joints. During strong earthquakes, relative large cyclic displacements may occur between the walls of rock joints. These cyclic displacements can degrade the first and second order asperities along the joint surface and reduce the shear strength of rock joint (Hosseinu et al., 2004).

Chen et al. (2003) studied the landslide history of Tsao-Ling by the pseudo-static stability analysis and found that the earthquake is the main factor of the landslide. The dynamic shear strength of rock joints which may cause by blasting or earthquakes is important for rock structures design. Nguyen (2013) performed the direct shear test on the rough joint surface of schistose rock blocks obtained from Mayen-Koblenz, Germany. The results show that peak shear stress under dynamic loading is approximately 30% higher than that under static loading and tent to increase with time.

During an earthquake, the cementation may be broken, asperities may be broken, or asperities may be overridden leading to non-fitting roughness patterns, all resulting in a cohesion and friction that are permanently reduced. Hence, an earthquake does not only add unfavorable forces to a slope but may also permanently reduce the shear strength along the discontinuity planes in a slope (Hack et al., 2007).

Even though the extensive study has been carried out in an attempt to understand the shear behavior under dynamic loading on single shear joint, the effect of dynamic loading on the shear strength of double rock joint is also needed to study. This is because in real rock mass, adjacent joints may interact with each other, and therefore the shear behavior of double rock joints may be very different from that of a single joint (Liu et al., 2017)

1.2 Research objective

The objective of this study is to determine the effects of earthquake vibration on the fracture shear strengths. Shear behavior of rock joints was investigated under double shear fracture with a constant normal load and dynamic boundary conditions. The experiments are conducted on smooth surface and rough joints in sandstone. The effects of normal stress and ground vibration (one-dimensional acceleration) on the shear behavior of rock joints were also investigated. The mathematical relations between shear parameters of rock joints and vibration effect was developed.

1.3 Research methodology

The research methodology shown in Figure 1.1 comprises 6 steps; including literature review, sample preparation, laboratory setting, Development of Mathematical Relation, discussions and conclusions and thesis writing.

1.3.1 Literature review

Literature review is carried out to understand the fractures shear strength under ground acceleration. These include theories, test procedures, results, analysis and applications. The sources of information are from journals, technical reports and conference papers. A summary of the literature review is given in the thesis.

1.3.2 Sample preparation

Rock samples used here have been obtained from the sandstone specimens from the Phra Wihan formations. Sample preparation will be carried out in the laboratory at Suranaree University of Technology. The specimens have been prepared to obtain

prismatic blocks and a test sample is divided into three phases on the top, the middle,

the bottom with nominal dimensions of $100 \times 100 \times 225$ mm^3.
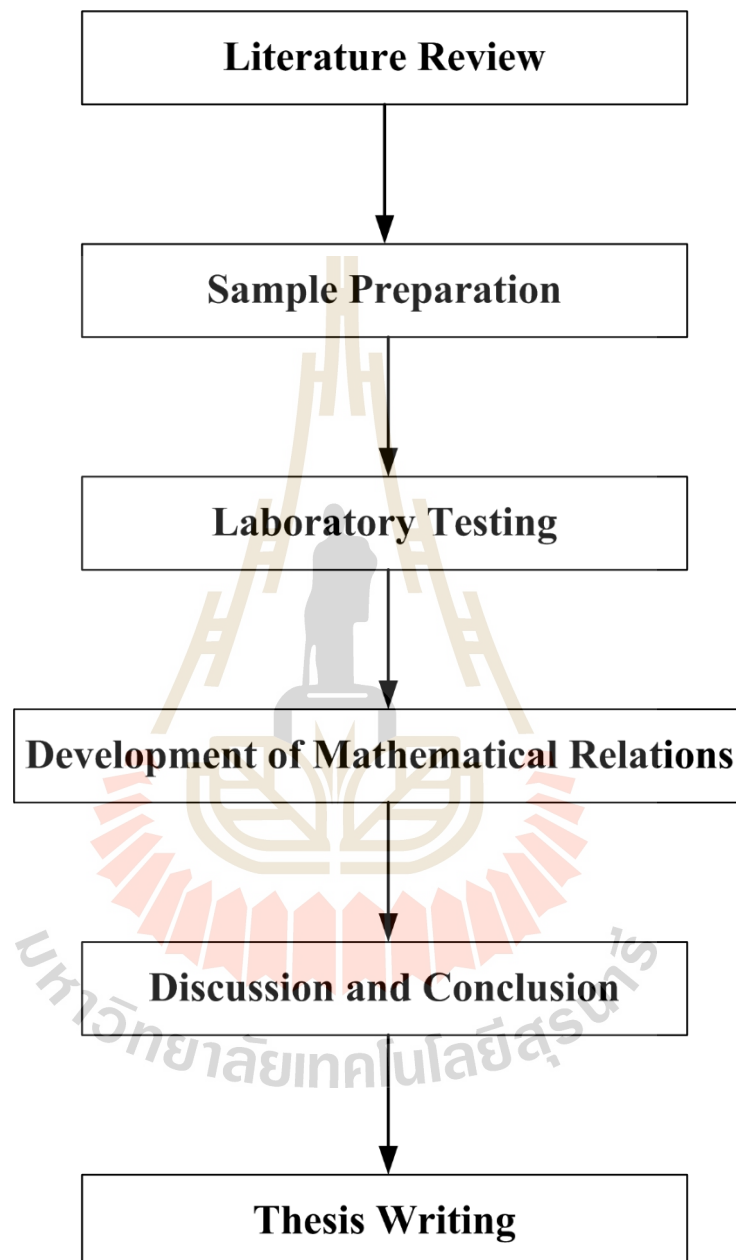
Figure 1.1 Research methodology.

1.3.3 Laboratory Testing

The test method uses double shear plane. The test is terminated when a total of 5 mm of shear displacement is reached. Double fracture shear test under is at constant normal loads (CNL). Figure 1.2 shows the positions of the direct shear device installed on acceleration device (shaking table). The normal loads will apply under four constant rates varying from 0.05 to 4.00 MPa. For the dynamic analysis, an actual measured earthquake acceleration time history in the north of Thailand has been scaled to provide peak ground acceleration values of 0.0 g to 0.8 g, which were converted to intensity of ground motion levels of I to VI (Seismological Bureau Thai Meteorological Department, 2014). These valves are estimated from the Mercalli scale (adapted from Richter, 1958 and Wald et al, 1999).

1.3.4 Development of Mathematical Relation

Results from laboratory test are used to formulate mathematical relations between the joint shear strengths, and normal stress. Such equation will be useful for determining the effect shearing resistance of functions under static and ground acceleration conditions.

1.3.5 Discussions and conclusions

Discussions and conclusions are made on the reliability and adequacies of the approaches used here. All research activities, methods, and results will be documented and complied with the thesis. The research or findings will be published in the conference.

1.3.6   Thesis writing

All research activities, methods, and results are documented and compiled in the thesis.

1.4   Scope and limitations of the study

The scope and limitations of the research include as follows.

1)   Laboratory testing follow the ASTM D5607 standards and recommendations of the ISRM.

2)   The direct shear testing is conducted under normal condition (static) and under vibration condition (ground acceleration) using the vibration table (shaking table).

3)   Up to 53 samples of Phra Wihan sandstone with nominal sizes of $100\times100\times225$ mm^3 are tested.

4)   The fractures of specimen are made in the laboratory by saw-cut and tension-inducing method.

5)   Direct shear tests are performed with constant normal stresses (σ_n) varying from 0.05 to 4.00 MPa.

6)   All tests are performed under ambient temperature.
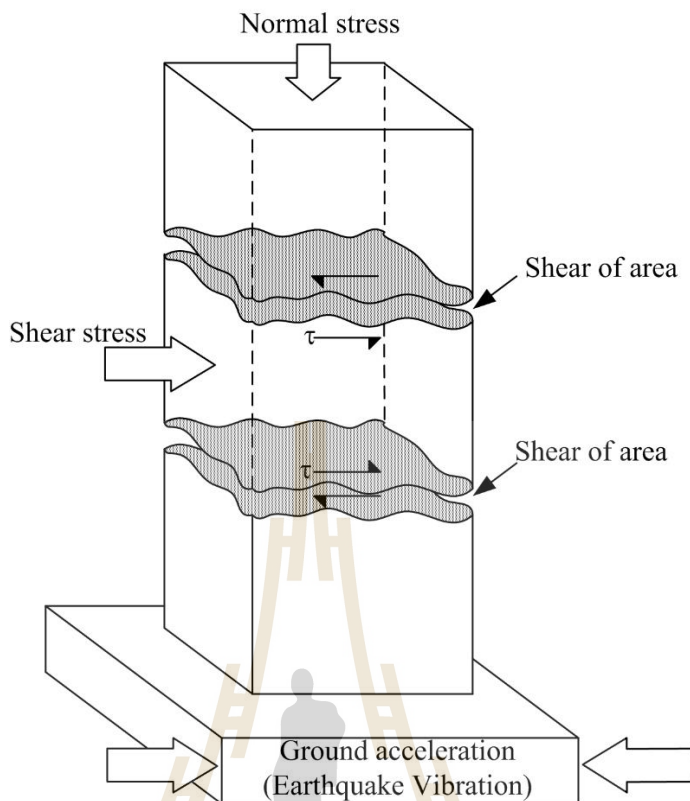
Figure 1.2 Test directly on Shear rock fracture (Direct Shear Testing Machine) and display concept Directors simulated seismic waves vibrate at different levels (Remember modified ASTM D5607).

1.5 Thesis contents

Chapter I introduces the thesis by briefly describing the background of problems and significance of the study. The research objectives, methodology, scope and limitations are identified. **Chapter II** summarizes results of the literature review. **Chapter III** describes the sample preparation **Chapter IV** presents the new design device. **Chapter V** presents the laboratory experiment. **Chapter VI** developed mathematic relations. **Chapter VII** are discussion and concludes the research results and provides recommendations for future research studies.

CHAPTER II

LITERATURE REVIEW

2.1 Introduction

This chapter summarizes the results of literature review carried out to understand the joint shear strength criteria, effect of shear rate and shear velocity, effect of joint roughness, effect of ground acceleration, effect of earthquake on geological structures and physical model simulation.

2.2 Joint Shear Strength Criteria

Coulomb criterion represents the relationship between the peak shear strength and normal stress by costs include costs of sample maintain, transport, prepares, and testing.

$$\tau = c + \sigma_n \tan\phi \qquad (2.1)$$

where τ is joint shear strength, σ_n is normal stress, c is the cohesive strength, and ϕ is angle of friction. These factors are the laboratory result. The result may not agree with rock mechanics work under high compressive strength. This is because of the relationship between τ and σ_n of Coulomb criterion is linear while actual relation is curve.

Barton (1973) has studied the behavior of natural rock joints and proposed a criterion that is modified from Patton. It can be re-written as

$$\tau = \sigma_n \tan \{\phi_b + JRC \log10 (\sigma_j/\sigma_n)\} \qquad (2.2)$$

where τ is joint shear strength, ϕ_b is basic friction angle, σ_n is normal stress, JRC is the joint roughness coefficient, and σ_j is the joint wall compressive strength. Joint roughness coefficient can correlate with Figure 2.1.
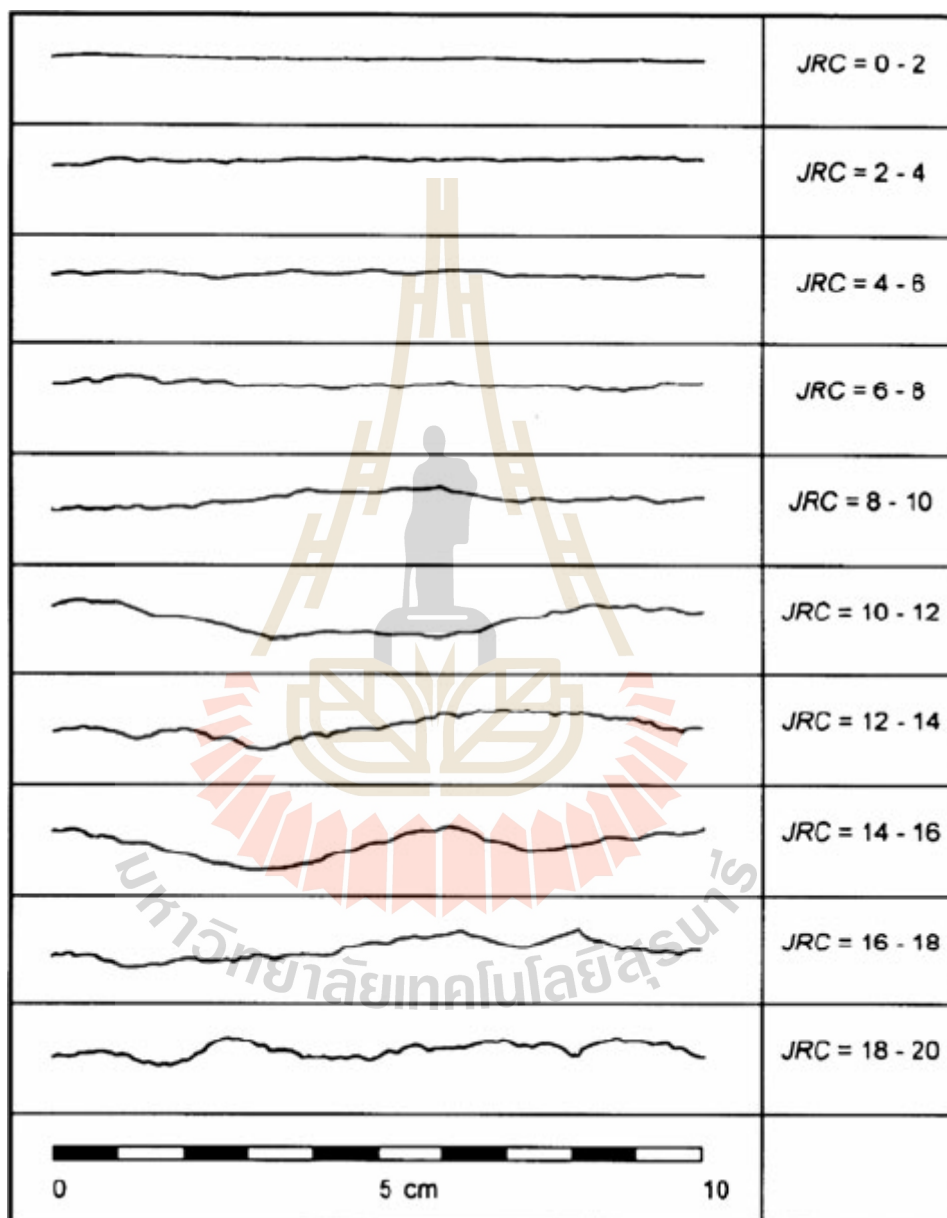
Figure 2.1 Roughness profiles and corresponding JRC values (Barton 1973).

2.3 Effect of shear rate and shear velocity

Frictional resistance of rock joints is dependent on the rate of shear displacement. The magnitude of this effect is quite variable, depending mainly on the rock type and normal stress level. In general, for harder rocks, the frictional resistance has been found to decrease with increasing shear displacement rates greater than a variable critical velocity (Crawford and Curran, 1981).

Jafari et al. (2003) have studied the effects of displacement rates (or shearing velocity) on shear strength, some monotonic tests were performed in different ranges of axial displacement in 4 MPa confining pressure from 0.05 to 0.4 mm/s. The differences between the curves can be related to the effects of shear velocity on second-order asperities, as the total applied displacement is limited. It is observed that shear strength reduces with increasing shear velocity, approaching the same values for the peak and residual strength at higher shearing velocities.

Park and Song (2009) perform direct shear test on a rock joint using a bonded particle model. The normal stresses applied to the sample were 3 and 15 MPa, which are approximately 2% and 10% of the uniaxial strength of the intact sample, respectively. The shear stress increased rapidly until the peak strength was passed, and reached some residual value that remained constant as the displacement continued. The peak and residual strengths were 5.33 and 1.82 MPa at low normal stress and 15.5 and 5.77 MPa at high normal stress. The friction calculated from the ratio of the peak shear strength to the given normal stress was higher at lower normal stress: 1.78 at 3 MPa and 1.03 at 15 MPa. The rate of change in normal displacement showed a maximum value at the peak shear stress level and decreased gradually in both cases. The normal displacement continued to increase at low normal stress, while it convergedat high

normal stress when the residual state reached. The normal displacements at a shear displacement of 1.6 mm were 0.795 mm at 3 MPa and 0.434 mm at 15 MPa. These are approximately 2.21% and 1.21% of the sample height of 36 mm, respectively. There were a larger number of normal cracks (tensile cracks) 8 than the shear cracks, and the total number increased with increasing normal stress: 650 cracks at 3 MPa and 3290 at 15 MPa. For reference, the number of joint contacts was 5,196 at the initial stage. The cracks were initiated at 80% of the peak (pre-peak), and propagated rapidly until the shear stress reached 80% of the peak stress after passing the peak (post-peak). After the first crack was initiated, the shear stress showed a non-linear relationship with the shear displacement.

2.4 Effect of Joint Roughness

Kwafniewski and Wang (1997) studied the surface roughness evolution and mechanical behavior of rock joints under shear. The shear behavior of rock joints characterized by the shear stiffness and peak shear strength depends mainly on the normal load applied. The shear stiffness and shear strength have relatively smaller values. Experiments show a complex dependence of shear stiffness and the peak shear strength on the roughness. The shear behavior of rock joints characterized by the shear stiffness and peak shear strength depends mainly on the normal load applied. Experimental results show that, at a lower θ, the shear stiffness and shear strength have relatively smaller values. In such a case, the shear resistance drops once the peak shear strength has been achieved. At a higher θ, however, both shear stiffness and the peak shear strength significantly increase and the drop in shear resistance after the peak shear strength becomes more evident. For θ = 45 °, i. e. high normal force conditions, a

number of significant peaks have been normally recorded in the post-initial yield region. When subjected to normal and tangential loads, the rough surfaces of rock joints experience damage in the process of shearing. The failure mode of asperities on the joint surfaces and the degradation of surface structure depend on the normal force applied as well as the shear history. The physical process of surface damage is in fact considerably complex. Due to the random character of surface structure, it is quite possible that the damage of a rough surface occurs as a result of several mechanisms. For instance, tensile split occurs at steeper asperities in one part, while sliding or rotation of failed asperities in another part of the joint. Moreover, in some sequences, individual mechanisms of surface damage may take place in the loading history. The observed macrochanges in the surface topography actually tell only a part of the story of the damage process.

Lee et al. (2001) proposed a cyclic shear testing system that is established to investigate the mechanical behavior of rough rock joints under cyclic loading conditions. Laboratory cyclic shear tests are conducted for two joint types of Hwangdeung granite and Yeosan marble, saw-cut and split tensile joints. Prior to the test, the roughness of each specimen is characterized by measuring the surface topography using a laser profilometer. Monotonic shear behaviors of rough joints are simulated using the proposed model in this study. Input parameters are obtained based on the results of laboratory tests. Initial asperity angles and damage coefficients are also calculated from the results of laser profilometer analysis and asperity degradations. Simulated shear behaviors of three rough joint specimens are superimposed on the laboratory test results. The proposed model precisely simulated the peak shear stresses and the shear stress–shear displacement relations from numerical simulations are

closely matched with the laboratory test results. Simulated dilation curves could also replicate the general trend of nonlinear changes for rough joint as discovered in the experimental results.

Kemthong and Fuenkajorn (2007) perform direct shear test on saw-cut specimens to determine the relationship between the basic friction angle (ϕ_b) and the rock compressive strength (UCS). Testing on specimens with tension-induced fractures yielded joint shear strengths under different JRC's for use in the verification. The results indicate that Barton's criterion using the field-identified parameters can satisfactorily predict the shear strengths of rough joints in marble and sandstones, and slightly over-predicts the shear strength in the basalt specimens. It cannot however describe the joint shear strengths for the granite specimens. This is probably because the saw-cut surfaces for coarse-grained and strong crystalline rocks are very smooth resulting in an unrealistically low ϕ_b. Barton's shear strength criterion is more sensitive to ϕb than to UCS and JRC. For all sandstones the ϕb values are averaged as 33 ± 8 degrees, apparently depending on their cementing materials. The average ϕb for the tested marbles and for the limestone recorded elsewhere 35 ± 3 degrees, and is independent of UCS. The ϕ_b values for other rock types apparently increase with UCS particularly for very strong rocks. The factors governing ϕ_b for crystalline rocks are probably crystal size, mineral compositions, and the cutting process, and for clastic rocks are grain size and shape and the strength of cementing materials.

2.5 Effect of ground acceleration

Terzaghi (1950) presented the pseudo-static method, which is a simple method for evaluating of seismic stability of a slope. This type of method can be used to man-

made or natural slopes based on either analytical method or numerical method. The earthquake force, acting on the an element or whole of the slope, is writed by a horizontal force and/or a vertical volum force equal to the gravitation force multiple a coefficient k, called the pseudo-static coefficient as shown in Figure 2.2 and Equation 2.3. Thus, k times the gravitational acceleration g, i.e. a = kg forms the assumed seismic acceleration a. The assumed pseudo-static forces acting on a potential sliding mass of weight W will be

$$f_h = \frac{a_h W}{g} = k_h W \ , \ f_v = \frac{a_v W}{g} = k_v W \qquad (2.3)$$

Where a_h and a_v are horizontal and vertical pseudo-static accelerations, respectively, k_h and k_v are horizontal and vertical pseudo-static coefficients, respectively.
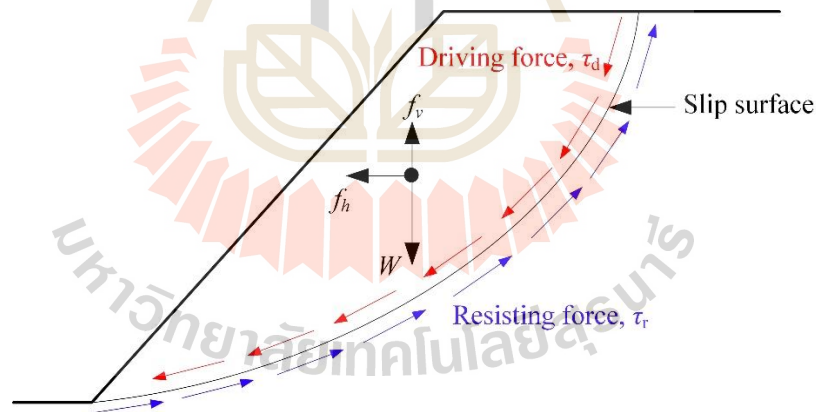
Figure 2.2 Forces acting on a slope in pseudo-static slope stability analysis

(Zhang 2015)**.**

The factor of safety (FOS) is represented as the ratio of the resisting force to the driving force, Equation (2.4).

$$FOS = \frac{\tau_r}{\tau_d} \hspace{4cm} (2.4)$$

From Equation (2.3), the pseudo-static force is determined by the seismic coefficient. The key problem for the pseudo-static procedure is how to select an appropriate seismic coefficient under an acceptable FOS. There have been studies for determining the most appropriate pseudo-static coefficient by a matter of experience and judgment. Classical paper made the original suggestion to use of $k_h = 0.1$ for severe earthquakes, $k_v = 0.2$ for violent and/or destructive earthquakes, and of $k_h = 0.5$ for catastrophic earthquakes.

Prasad et al. (2004) performed model testing under 1g environment in earthquake geotechnical engineering has become an integral part of research. When financial constraints exist, it is difficult to procure sophisticated shaking table. In such situations, manual shaking table can be fabricated and used. Fabricated shaking table generated 0.5 g level acceleration at around 2 Hz with a payload of 7 kN. It produced uni-axial, harmonic, sinusoidal vibration. The vibration frequency of shaking table depended on payload. A very low effort of around 80 N was sufficient to initiate and keep vibrating the table.

Baraza et al. (1992) analyzed of core samples from the western Alboran Sea slope reveal a large variability in texture and geotechnical properties. Stability analysis suggests that the sediment is stable under static gravitational loading but potentially unstable under seismic loading. Slope failures may occur if horizontal ground accelerations greater than 0.16 g and 0.43 g. are seismically induced.

Chen et al. (2003) studied extensive slope failures are triggered by the earthquake in central Taiwan. They used pseudo-static analysis. Pseudo-static stability analysis is performed with material properties degrading from peak strength to residual

strength and various reduction factors of peak ground acceleration. Based on the results of a pseudo-static analysis, the reduction factor of 2/3 appeared to be satisfactory for causing sliding with 30% degradation of material strength.

For historical earthquakes with no seismograph records, seismologists can estimate the intensity of ground motion from the Mercalli scale (Table 2.1), using the information as a kind of crude seismograph. If intensity information is available for enough different places, a rough estimate of the earthquake magnitude can be made (Gendzwill, 2008).

Table 2.1 Intensity of ground motion is estimated from the Mercalli scale

(Adapted from Richter, 1958 and Wald et al. 1999).

Modified Mercalli Intensity	Acceleration (g)	Description of Intensity Level
I	<0.0017	Not felt except by a very few under especially favorable circumstances.
II	0.0017	Felt only by a few persons at rest, especially on upper floors of buildings. Delicately suspended objects may swing.
III	0.014	Felt quite noticeably by persons indoors, especially on upper floors of buildings. Many people do not recognize it as an earthquake. Standing motor cars may rock slightly. Vibration similar to the passing of a truck. Duration estimated.
IV	0.014 – 0.039	Felt indoors by many, outdoors by few during the day. At night, some awakened. Dishes, windows, doors disturbed; walls make cracking sound. Sensation like heavy truck striking building. Standing motor cars rocked noticeably.
V	0.039 – 0.092	Felt by nearly everyone; many awakened. Some dishes, windows broken. Unstable objects overturned. Pendulum clocks may stop.

Table 2.1 Intensity of ground motion is estimated from the Mercalli scale

(Adapted from Richter, 1958 and Wald et al. 1999) (continued).

Modified Mercalli Intensity	Acceleration (g)	Description of Intensity Level
VI	0.092 – 0.18	Felt by all; many frightened. Some heavy furniture moved; a few instances of fallen plaster. Damage slight.
VII	0.18 – 0.34	Damage negligible in building of good design and construction; slight to moderate in well-built ordinary structures; considerable damage in poorly built or badly designed structures; some chimneys broken. Noticed by persons driving motorcars.
VIII	0.34 – 0.65	Damage slight in specially designed structures; considerable in ordinary substantial buildings with partial collapse. Damage great in poorly built structures. Fall of chimneys, factory stacks, columns, monuments, walls. Heavy furniture overturned.
IX	0.65 – 1.24	Damage considerable in specially designed structures; well-designed frame structures thrown out of plumb. Damage great in substantial buildings, with partial collapse. Buildings shifted off foundations.
X	> 1.24	Some well-built wooden structures destroyed; most masonry and frame structures destroyed with foundations. Rails bent.
XI	> 1.24	Few, if any (masonry) structures remain standing. Bridges destroyed. Rails bent greatly.
XII	> 1.24	Damage total. Lines of sight and level distorted. Objects thrown into the air.

Silva et al. (2006) stated that the horizontal ground acceleration varied from 0.07 g – 0.16 g for the neotectonic fault at the Gbraltar Strait tunnel area, Bolonia Bay (South Spain). Peak horizontal ground accelerations measured in the area Loma Prieta earthquake ranged between 0.1 and 0.25 g (Brune et al. 1991).

Hack et al. (2007) suggest that during the earthquake, the horizontal acceleration adds an unfavorably oriented force to the blocks that may cause instability. However,

the acceleration also reduces normal stresses on the contact plane and thereby the contribution of the friction to the shear strength along the plane.

Woodward and Griffiths (1996) Suggested pseudo-static and dynamic non-linear finite element analyses have been performed to assess the dynamic behaviour of gravity retaining walls subjected to horizontal earthquake loading. In the pseudo-static analysis, the peak ground acceleration is converted into a pseudo-static inertia force and applied as a horizontal incremental gravity load. In the dynamic analysis, an actual measured earthquake acceleration time history has been scaled to provide peak ground acceleration values of 0.1 g and 0.3 g. Good agreement is obtained between the pseudo-static analysis and analytical methods for the calculation of the active coefficient of earth pressure. However, the results from the dynamic analysis require careful interpretation. In the pseudo static analysis, the increase in the point of application of the resultant active force with the horizontal earthquake coefficient k_h from the one-third point to the mid-height of the wall is clearly observed. In the dynamic analysis, the variation in the point of application is shown to be a function of the type of wall deformation. Both finite element analyses indicate the importance of determining the magnitude of the predicted displacements when assessing the behaviour of the wall to seismic loading.

2.6 Effect of earthquake on geological structures

Owen and Scholl (1981) discussed a review of the past performance of 127 underground openings during earthquakes indicates that underground structures in general are less severely affected than surface structures at the same geographic location. However, some severe damage, including collapse, has been reported.

Stability of tunnels during seismic motion is affected by peak ground motion parameters, earthquake duration, and type of support, ground conditions, and in-situ stresses.

Daisuke et al. (2003) state that generally, underground caverns are highly resistant to earthquake. However, the underground cavern for the public use will be constructed in the ground with shallow overburden for convenience of access to the cavern. Therefore, in construction of underground rock cavern, influence of earthquake must be considered.

Hashash et al. (2001) suggested that performance of underground facilities during seismic events: (1) Underground structures suffer appreciably less damage than surface structures. (2) Damage from earthquake decreases with increasing overburden depth. Deep tunnels seem to be safer and less vulnerable to earthquake shaking than are shallow tunnels.

CDMG (1997) has developed the following guidelines on likely slope behavior; (1) 0–100 mm displacement-unlikely to correspond to serious landslide movement; (2) 100-1000 mm-slope deformations may be sufficient to cause serious ground cracking or enough strength loss to result in continuing post-seismic failure; and (3) More than 1000 mm displacement-damaging landslide movement and slopes should be considered unstable. When applying these displacement criteria in rock slope design, consideration should be given to the amount of displacement that will have to occur before the residual shear strength is reached. For example, if the sliding surface is a single discontinuity surface containing a weak infilling, a few centimeters of movement may be sufficient for the strength to be reduced to the residual value. In contrast, a fractured

rock mass may undergo several meters of displacement with little reduction in shear strength.

Ghosh et al. (1996) suggested that deep underground excavations are relatively more resistant to seismic loading from a single seismic event than are surface structures.

Dowding and Rozen (1978) presented one of the first compilations of damage to rock tunnels due to earthquake shaking. They collected information on 71 tunnels and compared their behavior with estimated peak ground accelerations (PGAs) and peak ground velocities (PGVs). Their conclusions can be summarized as follow; (1) Collapse of tunnels from shaking occurs only under extreme conditions. (2) No damage occurred when PGAs were lower than 0.19 g and/or PGVs were lower than 0.2 m/s. (3) Minor to moderate damage occurred when PGAs were up to 0.5 g and PGVs up to 0.9 m/s. (4) Moderate to heavy damage occurred when PGAs were larger than 0.5 g. (5) Tunnel collapse only occurred associated with movement of an intersected fault. (6) Tunnels are much safer than above ground structures for any given event.

Lenhardt (2009) suggested that effects on mining operations from earthquake loads need to be differentiated. Surface operations are much more likely to be affected earthquakes than underground workings, however. This principle applies worldwide. The situation in Austria is less serious, though, as seismic magnitudes of earthquakes are rather small to cause damage and thus pose a danger underground.

2.7 Physical models simulation

Barton and Hansteen (1979) used two-dimensional finite element continuum analyses and discontinuous physical models (20,000 discrete blocks) to compare the deformation resulting from the excavation of very large openings. They varied both

the joint orientations and the model horizontal stress levels are varied. Some models are dynamically loaded to simulate earthquakes (0.2-0.7 g). They state that high horizontal stress caused surface heave when joint orientations are favorable for arch stability. Joint orientations also determined whether the pillars between parallel openings are in a state of compression or tension.

Sakulnitichai et al. (2009) suggest that at shallow depths the acceleration can affect the underground excavation and the impact of the dynamic loads however reduces as the depth increases.

Genis and Aydan (2002) have used the dynamic shaking table tests as a tool in modeling of shallow opening. In model test, they used saw-cutting surface of Ryukyu limestone blocks. The geometry of the openings is rectangular (W/H=2/3) and square in cross-section since they are the optimum shapes in view of the existence discontinuity sets and gravitational loading. Four different conditions were investigated by considering the orientation of bedding planes and discontinuity patterns. There was no unstable block around the opening during and after shaking.

(a) Horizontal Model   (b) 30° inclined Model

(c) 60° inclined Model   (d) 60° inclined Model
(continuous joint)   (intermittent joint)
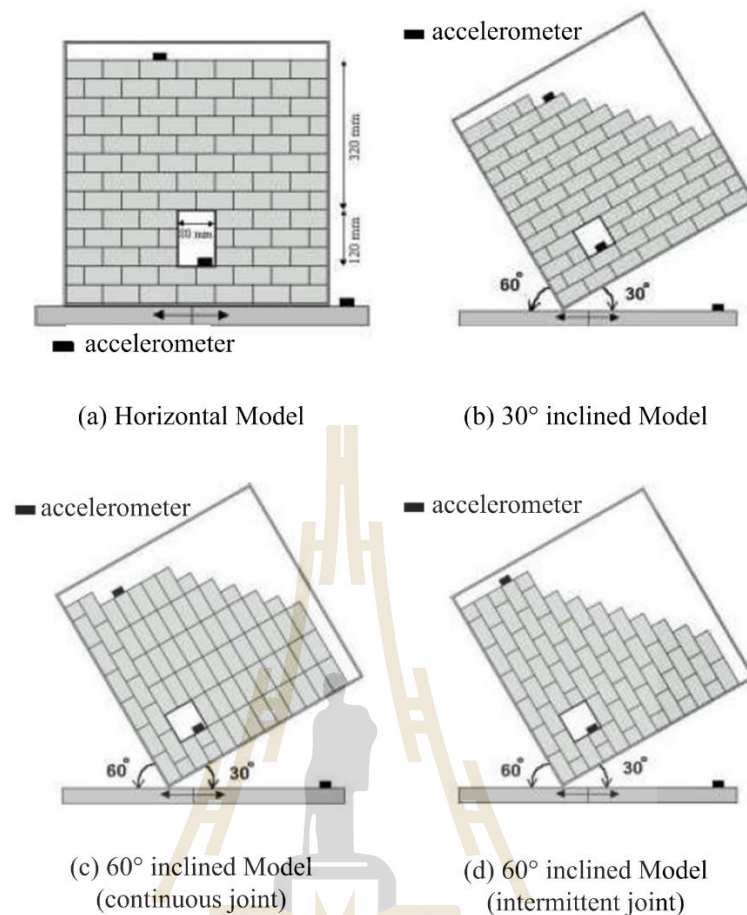
Figure 2.3 The model tests of underground openings on the shaking table (Genis and Aydan, 2002).

Pangpetch and Fuenkajorn (2007) used physical models or scaled-down models to simulate the failure behavior of rock slope in the laboratory. The design objectives are that it must be capable of simulating sliding and toppling failures under both dry and submerged conditions, and should allow assessing the effects of dynamic load lateral static acceleration on the slope stability. Figure 2.4 shows the test platform with block samples loaded inside the test frame. The simulation results indicate that the deterministic method of Hoek and Bray overestimates of plane sliding by as much as 30%. The observed toppling failures agree well with those determined by Hoek and Bray solution when the friction between blocks is considered in the calculation.

Kleepmek and Fuenkajorn (2013) performed scaled-down physical models are used to simulate slope failure formed by jointed rock mass. The tests aim to assess the effects of joint spacing and joint angle on the slope stability. Results indicate that plane sliding occurs when the slope are gentle and low with large joint spicing while combination of circular and plane sliding modes is observed when the slopes are steep and high with small joint specing. The results are compared with those obtained from the Hoek and Bray's solution, simplified Bishop method and UDEC simulations.
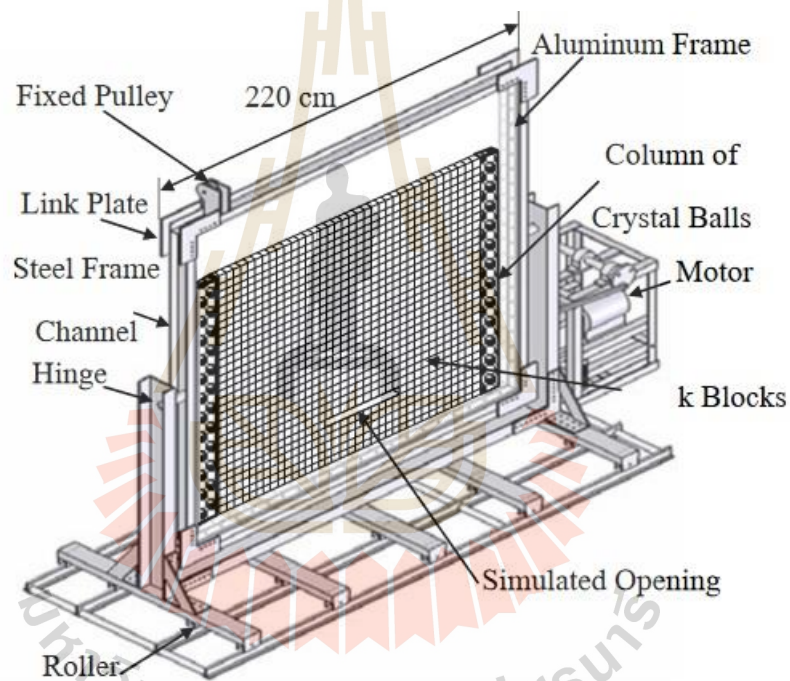
Figure 2.4 Test frame used in physical model (Pangpetch and Fuenkajorn, 2007).

CHAPTER III

SAMPLE PREPARATION

3.1 Introduction

The specimens used for the series of double fracture shear test are prepared from the sandstone specimens of the Phra Wihan formation. These rocks are classified as fine-grained quartz sandstones with highly uniform texture and density. They are well sorted and angular. The rock comprises 75% quartz (0.1-0.5 mm), 15% feldspar (0.2-0.5 mm), 7% mica (0.1-0.5 mm), 3% rock fragments (0.1-1 mm) (Kemthong and Fuenkajorn, 2007). These rocks have significant impacts on stability of many engineering structures constructed in Thailand (slope embankments, underground mines and tunnels). Sample preparation is carried out in the laboratory at the Suranaree University of Technology.

3.2 Sample preparation

Sixty-nine specimens are prepared for each test. Specimens for shear test are prepared to have fractures area of about 100×100 mm^2. The fractures are artificially made in the laboratory by saw-cut and tension inducing in $100 \times 100 \times 225$ mm^3 (Table 3.1). Samples comprise 3 blocks. Each block has a dimension of $100 \times 100 \times 75$ mm^3 (Figure 3.1). The fractures are artificially made in the laboratory by saw-cut and tension-induced method as shown in Figure 3.2 and Figure 3.3. Their roughenss is observed and classified by comparing with a reference profiles given by Barton (joint

roughness coefficient-JRC, Barton, 1973).   Figure 3.4 shows the joint roughness of some rock samples.
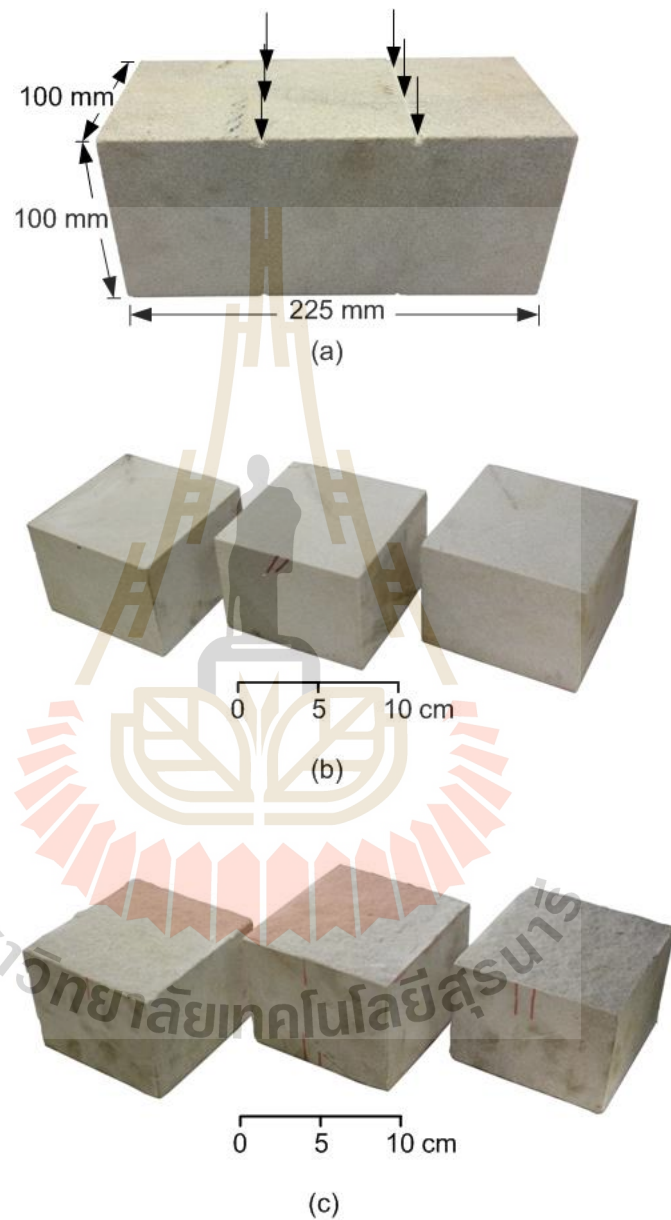
Figure 3.1   Sample preparation. (a) Some specimen before saw-cut/tension-induced

fracture, (b) Saw-cut fracture and (c) tension-induce fracture.

Figure 3.2 Saw-cut surface obtained from the saw machine.
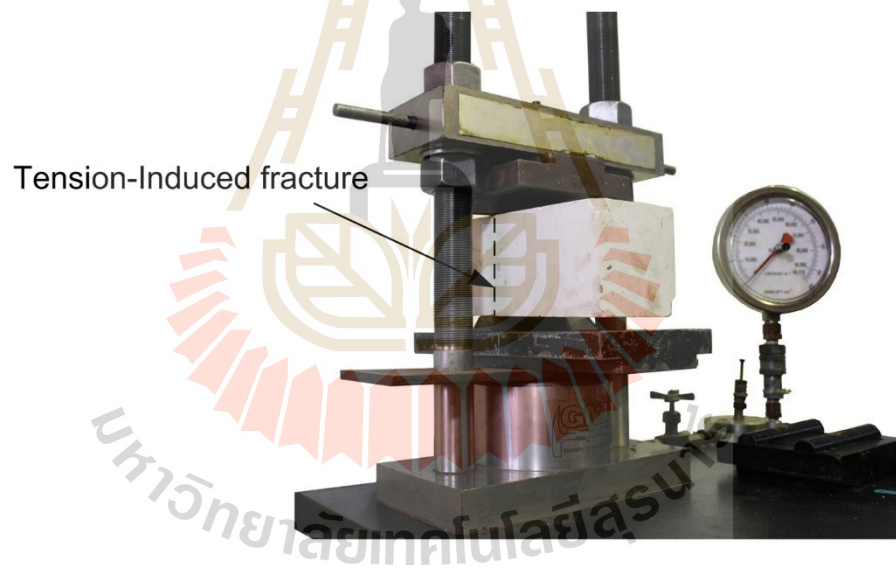
Figure 3.3 Line-load applied to obtain tension-induced fracture in sandstone fracture.
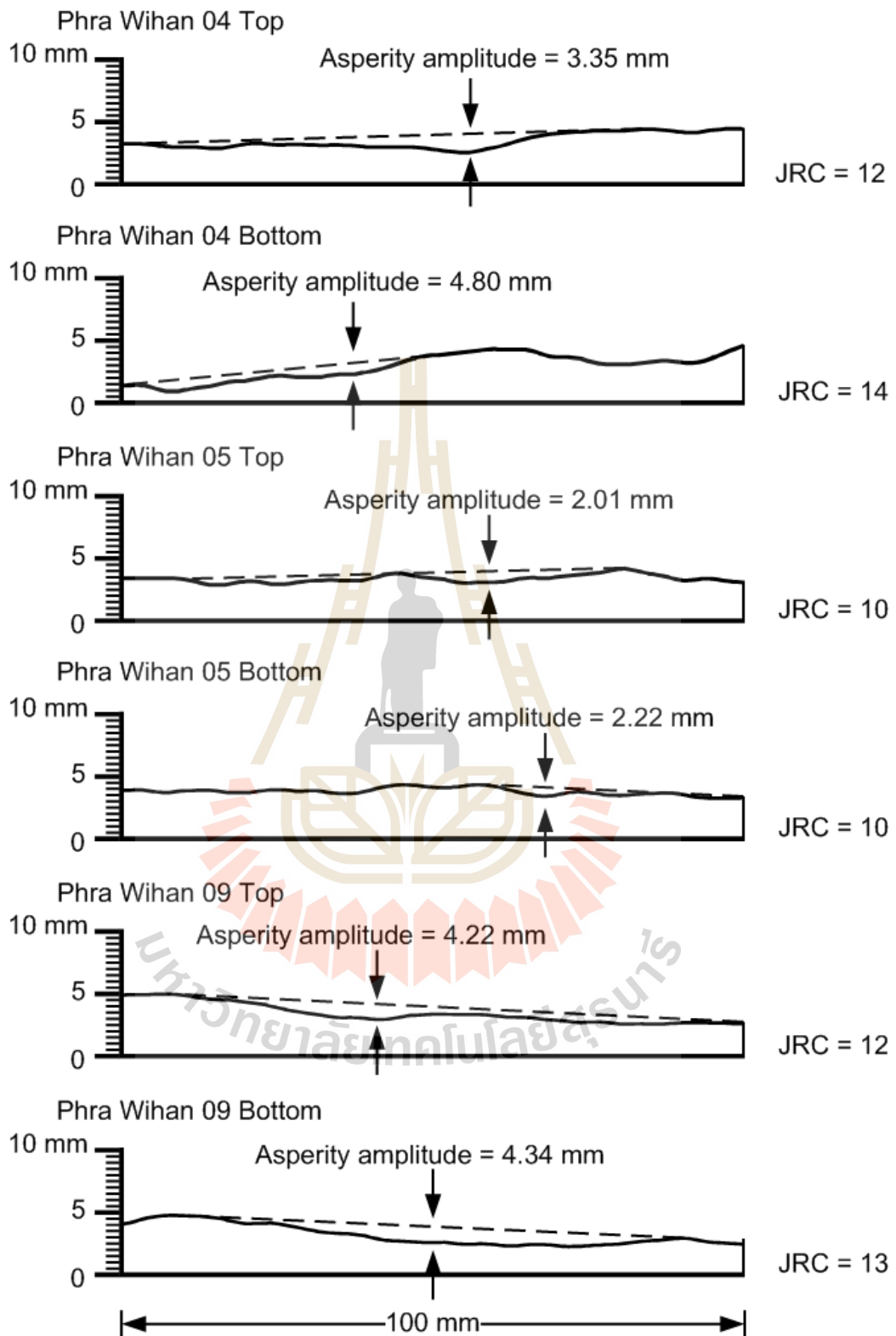
Figure 3.4 Some laser-scanned profiles to measure the maximum asperity amplitude

to estimate the joint roughness coefficient (JRC).

Table 3.1 Summary of Phra-Wihan sandstone specimens dimension of saw-cut and

tension induced fracture.

Specimen no.	Width (cm)	Length (cm)	Height (cm)	Double fracture area (cm^2)	Weight (g)	Density (g/cc)	JRC	
							Top	Bottom
PW-01	10.3	11.1	22.9	230.0	6155.54	2.35	0	0
PW-02	11.3	10.7	23.0	241.8	6335.02	2.28	0	0
PW-03	10.5	10.7	22.9	224.7	6213.23	2.34	0	0
PW-04	10.2	11.0	22.9	224.4	6261.32	2.36	0	0
PW-05	11.7	10.7	22.9	250.4	6499.85	2.30	0	0
PW-06	10.6	11.3	23.2	239.6	6331.12	2.28	0	0
PW-07	11.0	10.3	23.0	226.6	6231.61	2.39	0	0
PW-08	11.1	10.5	22.9	233.1	6261.32	2.36	0	0
PW-09	11.2	11.8	22.7	265.4	6755.35	2.32	0	0
PW-10	11.1	10.6	23.0	235.3	6216.22	2.29	0	0
PW-11	11.2	11.3	23.1	253.1	6311.21	2.33	0	0
PW-12	11.2	11.3	23.1	253.1	6311.21	2.33	0	0
PW-13	10.9	10.9	23.2	237.6	6287.95	2.28	0	0
PW-14	10.2	11.0	22.9	224.4	6261.32	2.36	13	10
PW-15	13.0	10.5	22.9	273.0	6412.87	2.37	12	13
PW-16	11.7	10.1	22.9	236.3	6191.45	2.25	10	11
PW-17	11.3	10.7	23.0	241.8	6335.02	2.28	13	10
PW-18	10.3	11.1	22.9	230.0	6155.54	2.35	13	11
PW-19	11.0	11.5	22.9	253.2	6332.28	2.25	12	11
PW-20	11.1	10.7	23.1	237.5	6263.38	2.28	11	13
PW-21	11.3	10.6	22.7	239.6	6216.22	2.29	13	12
PW-22	10.9	10.9	23.2	237.6	6287.95	2.28	12	12
PW-23	10.2	11.3	23.1	230.5	6107.83	2.29	12	10
PW-24	11.8	10.2	23.2	240.7	6356.93	2.28	11	12
PW-25	11.5	10.7	22.9	246.1	6405.84	2.34	10	11

Table 3.1 Summary of Phra-Wihan sandstone specimens dimension of saw-cut and

tension induced fracture (continued).

Specimen no.	Width (cm)	Length (cm)	Height (cm)	Double fracture area (cm^2)	Weight (g)	Density (g/cc)	JRC	
							Top	Bottom
PW-26	11.7	10.7	22.9	250.4	6499.85	2.30	13	11
PW-27	10.6	11.3	23.2	239.6	6331.12	2.28	13	10
PW-28	10.7	11.5	23.1	246.1	6453.05	2.27	12	10
PW-29	11.5	11.7	23.0	269.1	6365.55	2.32	11	11
PW-30	10.4	11.1	23.1	230.9	6311.88	2.29	12	11
PW-31	12.0	11.2	23.2	268.8	6421.66	2.25	12	10
PW-32	11.0	10.3	23.0	226.6	6231.61	2.39	11	13
PW-33	10.6	10.8	23.2	229.0	6122.54	2.31	13	11
PW-34	10.4	10.7	23.2	222.6	6234.22	2.41	13	10
PW-35	11.2	11.3	23.1	253.1	6311.21	2.33	11	13
PW-36	11.7	11.5	23.2	269.1	6422.81	2.28	12	11
PW-37	11.3	10.6	23.1	239.6	6308.14	2.28	11	10
PW-38	11.5	10.7	23.0	246.1	6429.45	2.27	13	10
PW-39	10.9	11.5	23.0	250.7	6530.93	2.27	12	11
PW-40	10.4	10.6	23.1	220.5	6124.52	2.41	11	13
PW-41	11.2	10.7	23.1	239.7	6310.80	2.35	12	10
PW-42	11.4	11.1	22.9	253.1	6322.25	2.32	12	11
PW-43	10.5	11.1	22.8	233.1	6223.22	2.32	11	12
PW-44	11.1	10.5	22.9	233.1	6261.32	2.36	12	13
PW-45	11.2	10.8	22.8	241.9	6412.87	2.37	11	12
PW-46	10.6	11.1	22.9	235.3	6191.45	2.25	13	12
PW-47	10.7	11.5	22.7	246.1	6335.02	2.28	11	12
PW-48	11.3	10.7	23.1	241.8	6155.54	2.35	13	11
PW-49	11.4	10.8	23.0	246.2	6332.28	2.25	12	11
PW-50	11.2	10.8	22.9	241.9	6263.38	2.28	13	11

Table 3.1 Summary of Phra-Wihan sandstone specimens dimension of saw-cut and

tension induced fracture (continued).

Specimen no.	Width (cm)	Length (cm)	Height (cm)	Double fracture area (cm^2)	Weight (g)	Density (g/cc)	JRC	
							Top	Bottom
PW-51	11.1	10.6	23.0	235.3	6216.22	2.29	12	12
PW-52	10.7	10.9	22.8	233.3	6287.95	2.28	13	11
PW-53	11.3	10.7	22.8	241.8	6107.83	2.29	11	12
PW-SC-01	11.6	11.1	22.7	258.7	6511.21	2.21	0	0
PW-SC-02	10.5	10.7	22.9	224.7	6422.81	2.50	0	0
PW-SC-03	11.2	11.8	22.7	265.4	6808.14	2.26	0	0
PW-SC-04	11.5	10.7	22.9	246.1	6429.45	2.28	0	0
PW-SC-05	11.7	10.7	22.9	250.3	6661.32	2.32	0	0
PW-SC-06	10.6	11.3	23.2	239.5	6412.87	2.31	0	0
PW-SC-07	10.7	11.5	23.1	246.1	6391.45	2.25	0	0
PW-SC-08	12.0	11.0	22.9	264.0	6753.05	2.23	0	0
PW-TI-01	11.6	11.1	22.7	258.7	6511.21	2.21	12	10
PW-TI-02	10.5	10.7	22.9	224.7	6422.81	2.50	11	11
PW-TI-03	11.2	11.8	22.7	265.4	6808.14	2.26	12	11
PW-TI-04	11.5	10.7	22.9	246.1	6429.45	2.28	12	10
PW-TI-05	11.7	10.7	22.9	250.4	6661.32	2.32	11	13
PW-TI-06	10.6	11.3	23.2	239.6	6412.87	2.31	13	11
PW-TI-07	10.7	11.5	23.1	246.1	6391.45	2.25	13	10
PW-TI-08	12.0	11.0	22.9	264.0	6753.05	2.23	12	10

CHAPTER IV

DOUBLE FRACTURE SHEAR TEST WITH SHAKING TABLE

4.1 Introduction

A double shear load frame with shaking table is fabricated to determine the effect of earthquake vibration on shear strength in rock joints. The direct shear testing is performed by using the Double fracture shear device which is installed on the shaking table. The testing is conducted under static and dynamics conditions. A new design of Double fracture shear device is aired to verify the performance of testing design with ASTM standard device. Therefore, the cohesion and friction angle between double fracture shear and SEBL DR-44 (Figure 4.1) devices are compared. This chapter describes the design requirements, the components of the double fracture shear and shaking table devices.

4.2 Design requirements and components

The functional requirements for the double fracture shear with earthquake condition are; (1) double fracture shear and (2) shaking table devices.

4.2.1 Double fracture shear device

Figures 4.2 through 4.4 show two steel cross load frames (horizontal axial load frame and vertical axial load frame), the main parts of the double fracture shear device (DFSD).
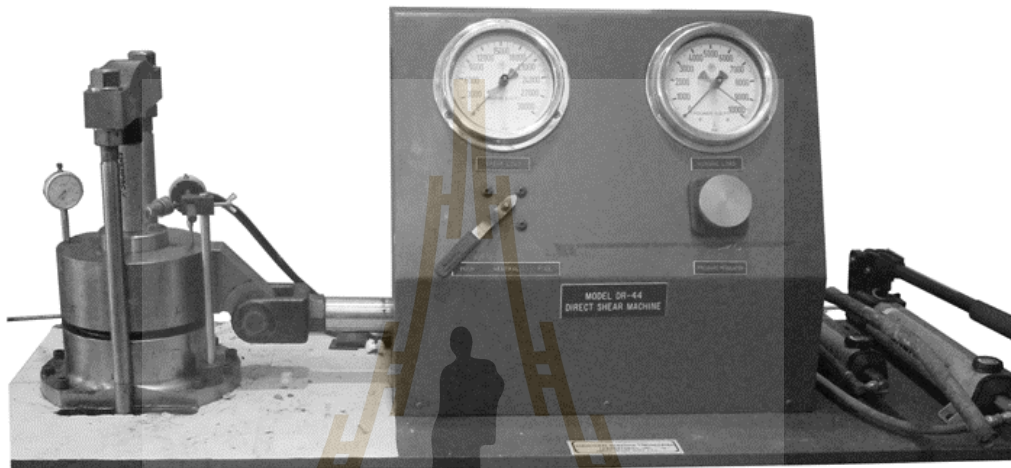
Figure 4.1 Direct shear test machine, SEBL DR-44 for standard ASTM D5607.
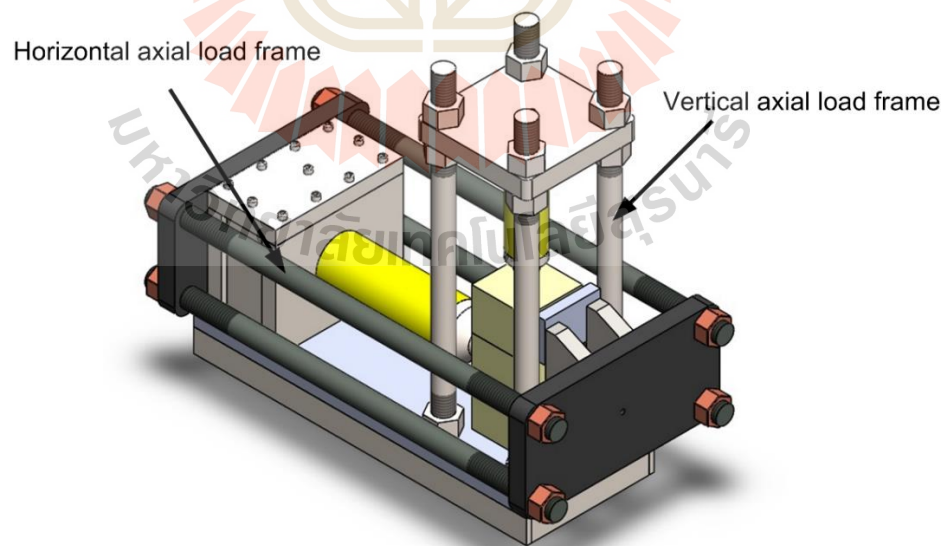
Figure 4.2   Two steel cross load frames (horizontal axial and vertical axial load frames).

Horizontal axial load frame

Vertical axial load frame
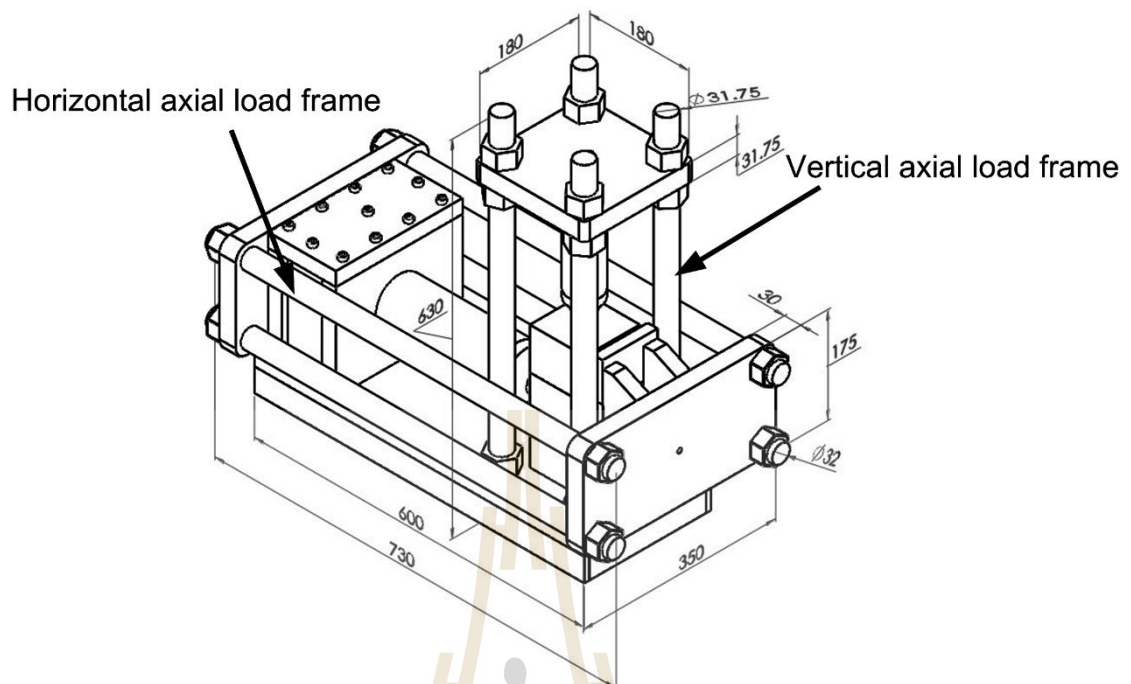
Figure 4.3 Two steel cross load frames (horizontal axial and vertical axial load frames) with dimension (mm).

Top view

Isometric

Front view

Right view

Bottom view

Isometric
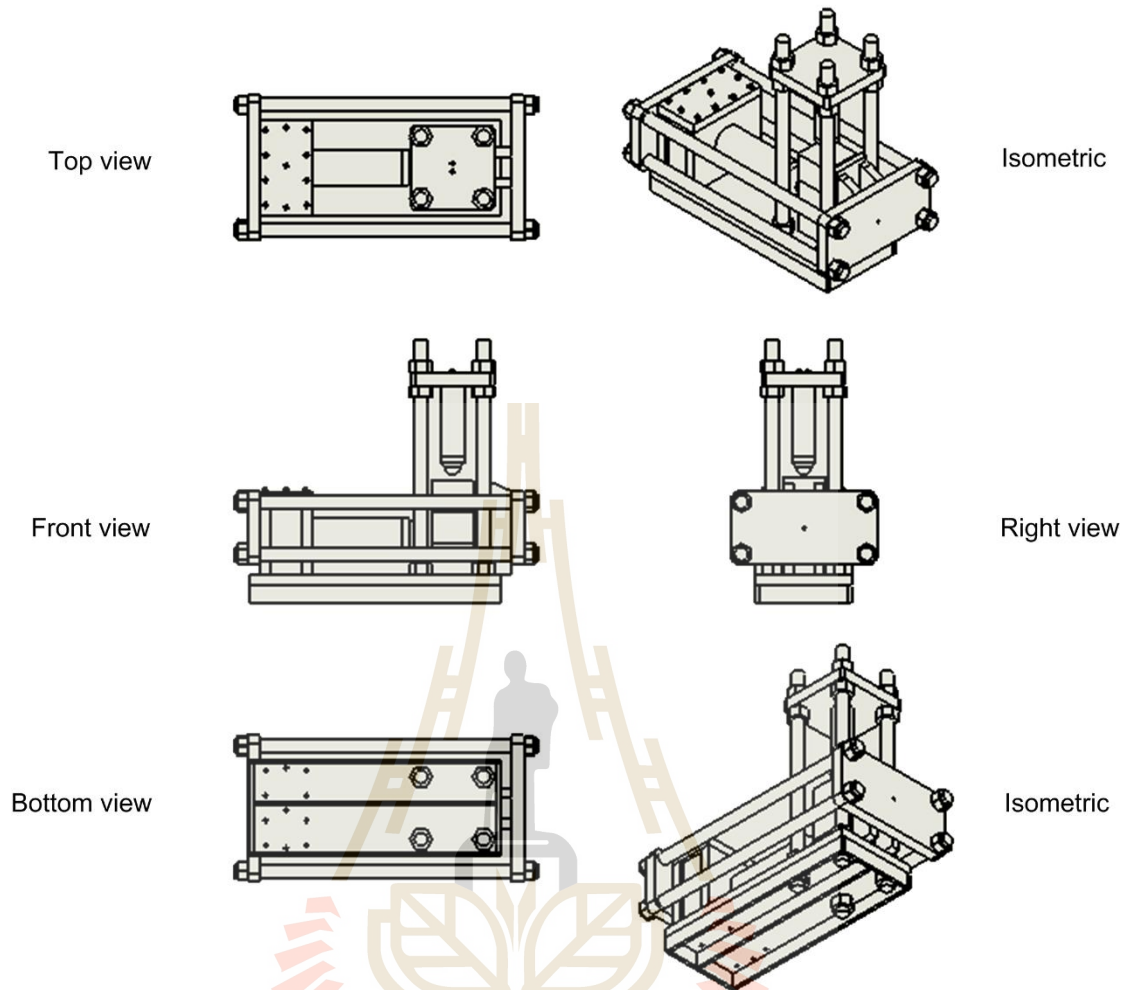
Figure 4.4 Two steel cross load frames (horizontal axial and vertical axial load frames) with multi-views section.

This device comprises three main components: two steel sets cross load frames, two hydraulic load cells and two hand pumps. Each load frame has two thick supporting steel plates, connected by four steel rods. They support the structures of the two load cells. The two load cells, installed at the supporting plates, are connected to two hand pumps with the capacity of 10,000 psi (Figure 4.5). Besides the three main parts, other accessories designed to measure and monitor the rock stresses and deformations during testing include two 4-inch pressure gauges and three dial gauges. The two pressure gauges are installed at two hand pumps to measure the applied load, while the three dial gauges measure the deformations along the principal axes for further strain calculation. Figure 4.6 shows typical picture of double fracture shear device during the direct shear test.
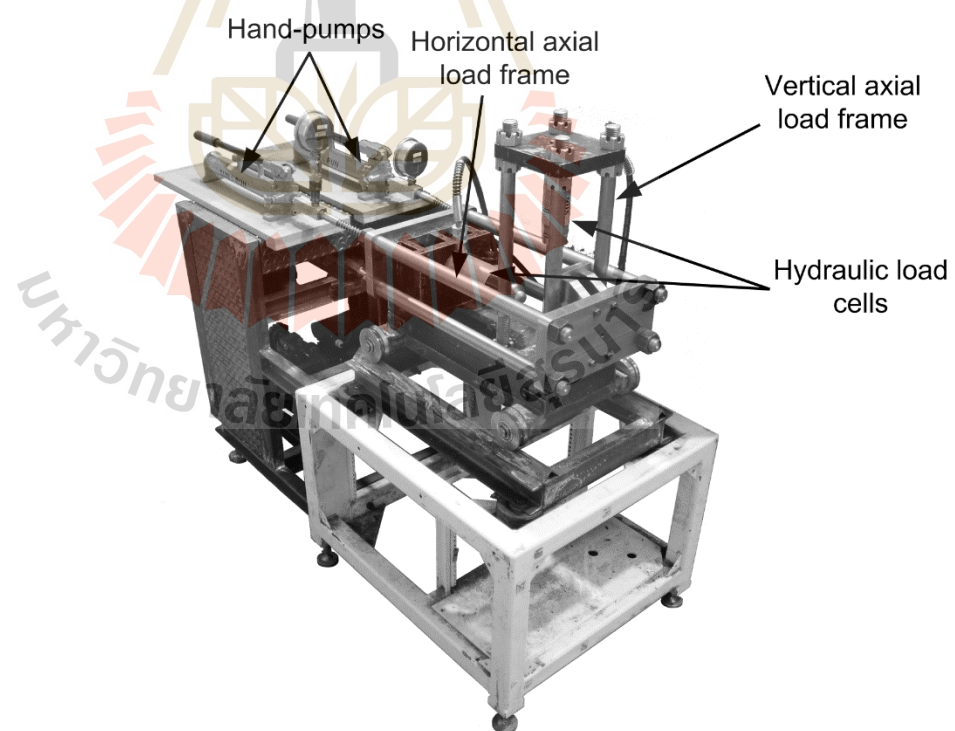
Figure 4.5   Components of double fracture shear device: main components and accessories.
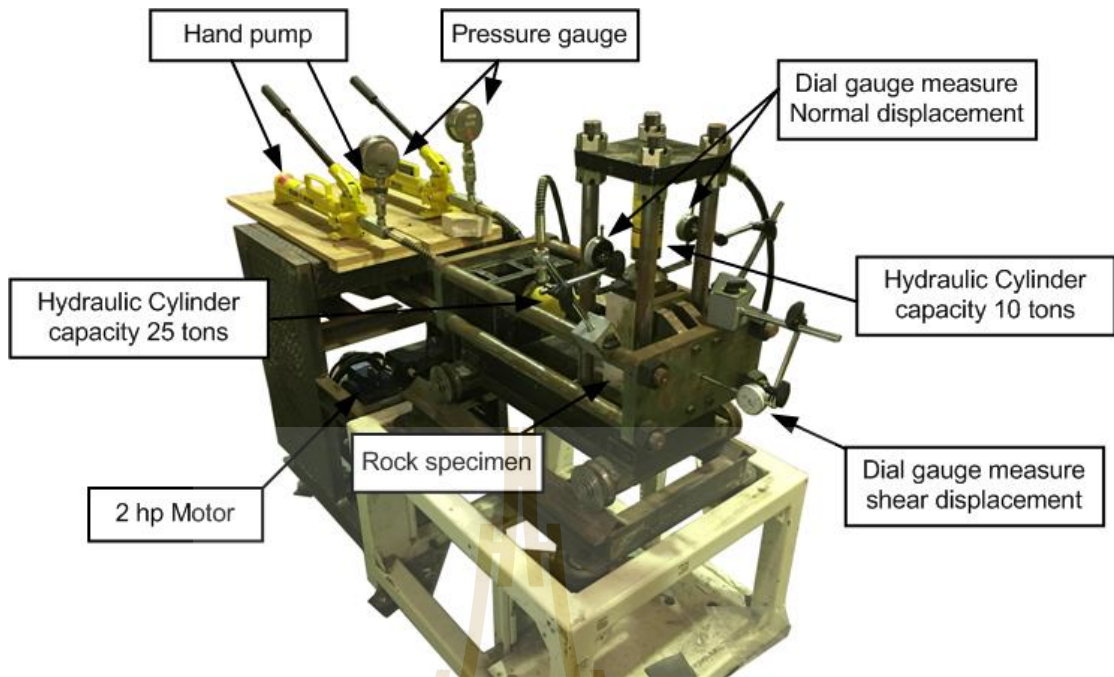
Figure 4.6 Typical picture of double fracture shear device during the direct shear test.

For the measure of force needed in the calibration process of the load cell and handheld data logger (Figure 4.7), only the psi and kilonewton units. The results of calibration of pressure gauge and hydraulic load cell are presented in Figure 4.8 and 4.9. Table 4.1 shows the results of calibration of pressure gauge and hydraulic load cell.

Figure 4.7 Load cell and handheld data logger.
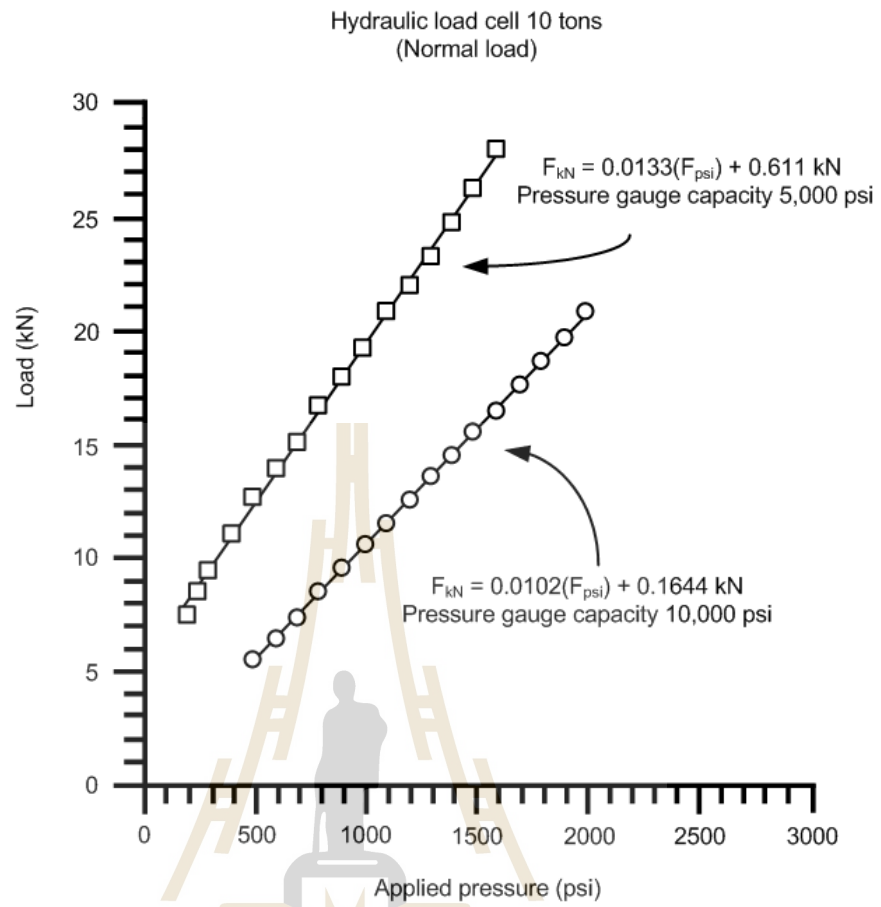
Figure 4.8   Results of calibration of pressure gauge and hydraulic load cell capacity
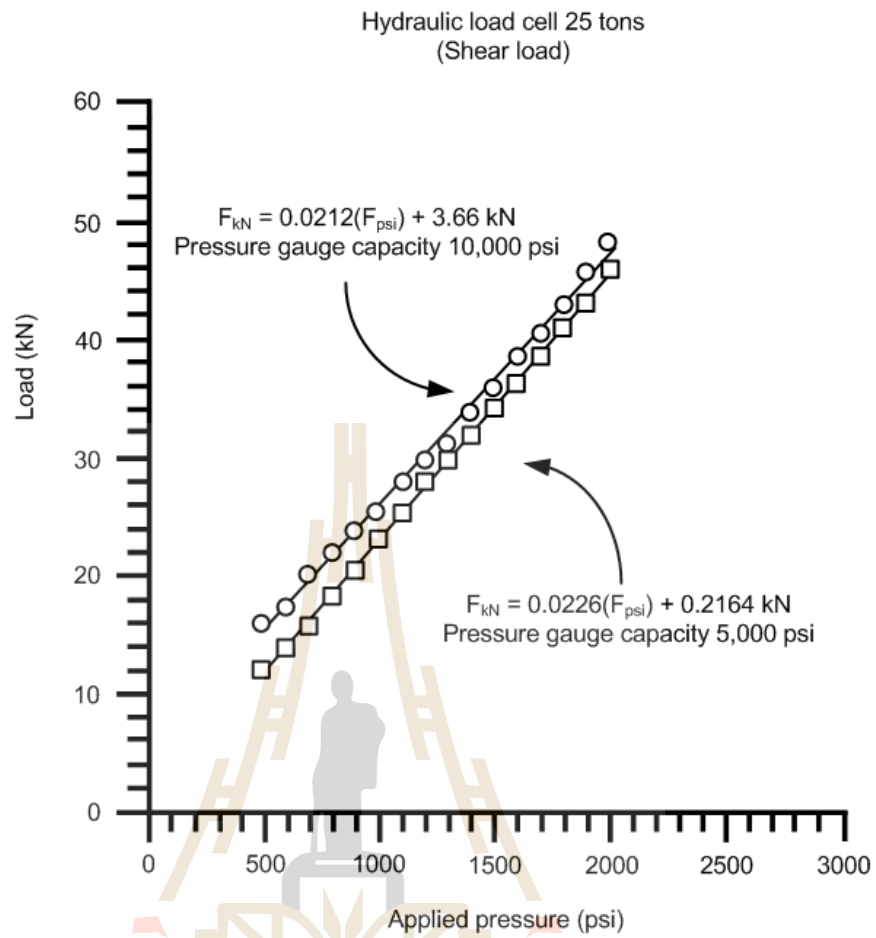
10 tons.

Figure 4.9   Results of calibration of pressure gauge and hydraulic load cell capacity

25 tons.

Table 4.1 Results of calibration of pressure gauge and hydraulic load cell

Hydraulic load cell capacity 10 tons (Normal load)				Hydraulic load cell capacity 25 tons (Shear load)			
Pressure gauge 5,000 psi		Pressure gauge 10,000 psi		Pressure gauge 5,000 psi		Pressure gauge 10,000 psi	
psi	kN	psi	kN	psi	kN	psi	kN
500	7.3	500	5.27	500	11.85	500	15.82
600	8.3	600	6.30	600	13.77	600	17.50
700	9.2	700	7.22	700	15.65	700	20.00
800	10.9	800	8.32	800	18.17	800	22.00
900	12.5	900	9.38	900	20.35	900	23.80
1,000	13.8	1,000	10.37	1,000	22.95	1,000	25.30
1,100	15.0	1,100	11.32	1,100	25.17	1,100	27.50
1,200	16.5	1,200	12.33	1,200	27.78	1,200	29.65
1,300	17.8	1,300	13.38	1,300	29.73	1,300	31.22
1,400	19.0	1,400	14.30	1,400	31.80	1,400	33.65
1,500	20.7	1,500	15.38	1,500	34.17	1,500	35.85
1,600	21.8	1,600	16.33	1,600	36.18	1,600	38.40
1,700	23.0	1,700	17.40	1,700	38.53	1,700	40.35
1,800	24.5	1,800	18.45	1,800	40.87	1,800	42.75
1,900	26.0	1,900	19.53	1,900	42.97	1,900	45.52
2,000	27.8	2,000	20.60	2,000	45.75	2,000	48.25

A new design of double fracture shear test device is aired to verify the performance of testing design with ASTM standard device. Therefore, the cohesion and friction angle between double fracture shear and SEBL DR-44 devices are compared. For verifying the reliability of the double fracture shear device test results above and to correlate the saw-cut shear strengths obtained from the two tests. The results of shear strength of both test machines are shown in Table 4.2. The results of cohesion and friction angle of both test machines are shown in Table 4.3. The results of comparison of saw-cut and roughness surface are presented in the forms of τ-σ_n diagrams in Figure 4.10. The results from the direct shear tests of sandstone from the two techniques are similar the rock sample of both test machines after testing as shown in Figures 4.11 and 4.12. The shear strengths of the smooth saw-cut fractures are also incorporated. Good correlations between the test results and the Coulomb criterion are obtained. The coefficient of correlations (R^2) for all curves are greater than 0.9.

Table 4.2 Summary of shear strength of compare devices.

Specimen No.	Fracture type	Device	Normal load (MPa)	Shear strength (MPa)
PW-SC-01	Saw-cut	DFSD	1	0.88
PW-SC-02	Saw-cut	DFSD	2	1.46
PW-SC-03	Saw-cut	DFSD	3	2.09
PW-SC-04	Saw-cut	DFSD	4	2.81
PW-SC-05	Saw-cut	SBEL DR-44	1	0.84
PW-SC-06	Saw-cut	SBEL DR-44	2	1.46
PW-SC-07	Saw-cut	SBEL DR-44	3	2.11
PW-SC-08	Saw-cut	SBEL DR-44	4	2.77
PW-TI-01	Tension-induce	DFSD	1	1.66
PW-TI-02	Tension-induce	DFSD	2	2.44
PW-TI-03	Tension-induce	DFSD	3	3.32
PW-TI-04	Tension-induce	DFSD	4	3.87

Table 4.2 Summary of shear strength of compare devices (continued).

Specimen No.	Fracture type	Device	Normal load (MPa)	Shear strength (MPa)
PW-TI-05	Tension-induce	SBEL DR-44	1	1.81
PW-TI-06	Tension-induce	SBEL DR-44	2	2.38
PW-TI-07	Tension-induce	SBEL DR-44	3	3.36
PW-TI-08	Tension-induce	SBEL DR-44	4	3.98

Table 4.3 Cohesion and friction angle of both test machines.

Devices	Conditions	Cohesion (MPa)	Friction angle (degree)	R^2
Double fracture shear	Saw-cut	0.21	33	0.99
	Roughness	0.92	37	0.99
SBELL DR-44 (ASTM D5607)	Saw-cut	0.19	33	0.99
	Roughness	1.01	37	0.98
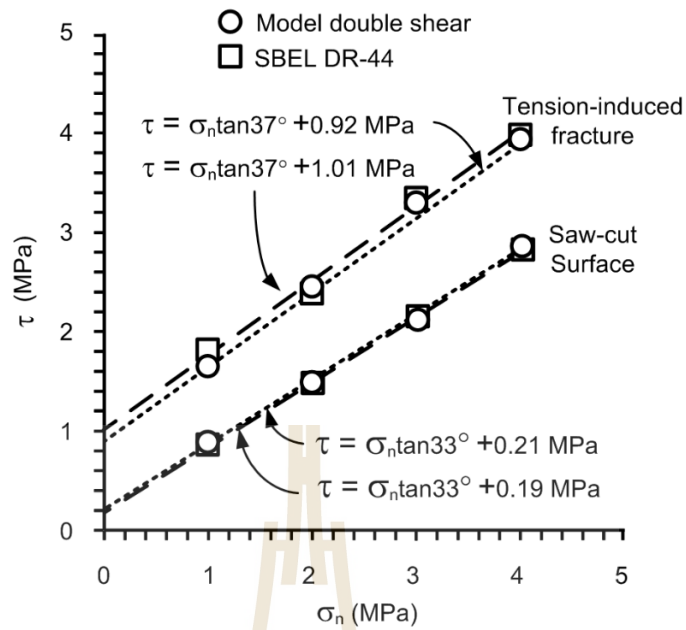
Figure 4.10 Shear strength as a function of normal stress of Phra Wihan sandstone compared between Double fracture shear device and ASTM standard device.
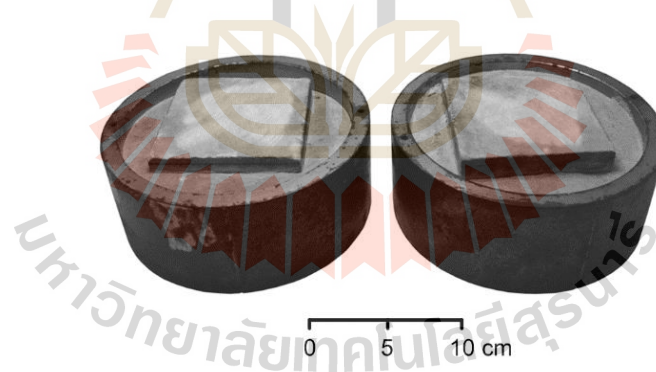
Figure 4.11 Some post-test saw-cut surface of SBEL DR-44 Device.
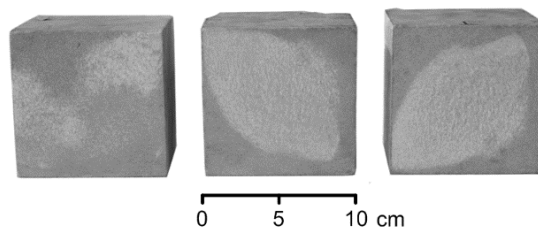
Figure 4.12 Selected post-test saw-cut surface of Double fracture shear device.

4.2.2 Shaking table device

The double fracture shear test device are installed on the shaking table. The effect of ground acceleration is studied by considering the effects of the horizontal pseudo-static acceleration induced by cyclic motions of the test platform in the direction parallel with the horizontal plane. These cyclic motions are used to simulate the earthquake shaking. Only the horizontal acceleration is simulated here because it has more impact on the geological structures than does the vertical acceleration (Kramer, 1996). Figure 4.13 shows the crank arm components used to generate the horizontal acceleration to the test frame. The acceleration at point B, represented by a, can be calculated using a set of equations given by Riley & Sturges (1993).

$$a = R\omega_{OA}^2 cos\theta + y\omega_{AB}^2 cos\phi - y\alpha_{AB} sin\phi \tag{4.1}$$

The angle ϕ can be obtained from

$$\phi = sin^{-1}\left[\frac{Rsin\theta}{y}\right] \tag{4.2}$$

The angular velocity (ω) of OA and AB can be calculated by

$$\omega_{OA} = \frac{2\pi}{T} \tag{4.3}$$

and

$$\omega_{AB} = \frac{R\omega_{OA}\,cos\theta}{y\,cos\phi} \tag{4.4}$$

The actual rotational duration (T) is monitored for each model hence changes the speed of the test platform and the flywheel rotation.

The relationship between point A and B, and α_{AB}, is calculated by:

$$\alpha_{AB} = \frac{R\omega_{OA}^2 \sin\theta - y\omega_{AB}^2 \sin\phi}{y\cos\phi} \qquad (4.5)$$

where R = radius of wheel, y = length of crack arm, ω_{OA} and ω_{AB} = angular velocity of OA and AB, θ = angle between AO and OB. α_{AB} = relationship between the acceleration of points A and B, and T = duration of flywheel rotation.
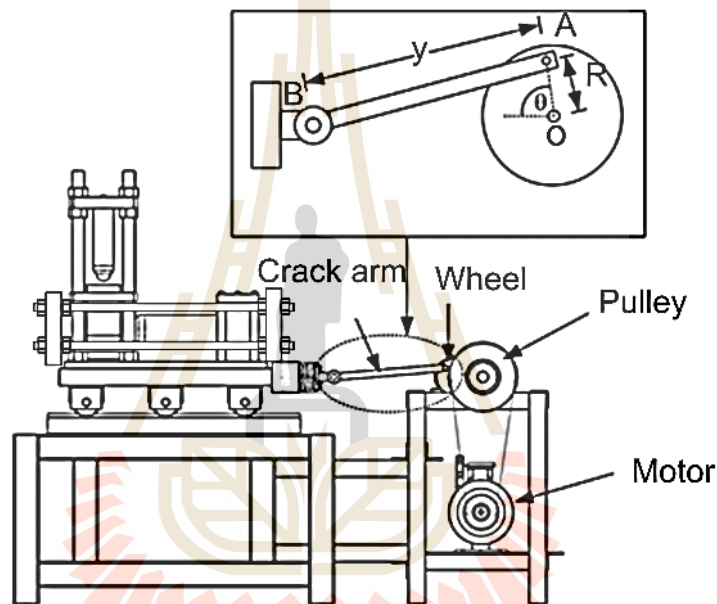
Figure 4.13 Crank arm and flywheel used to induce dynamic loading to the test platform.

Figure 4.14 shows spur gears are gears in the same plane that move opposite of each other because they are meshed together. Gear A is called the driver because this is turned by a motor. As gear A turns it meshes with gear B and it begins to turn as well. Gear B is called the driven gear. The cycle at gear B, represented by a, can be calculated using a set of equations.

$$\frac{N_{Driven}}{N_{Driver}} = \frac{n_{Driver}}{n_{Driven}} \tag{4.6}$$

where N_{Driven} = cycle of gear on the driven gear, N_{Driver} = cycle of gear on the driver gear, n_{Driver} = number of teeth on the driver gear, n_{Driven} = number of teeth on the driven gear.
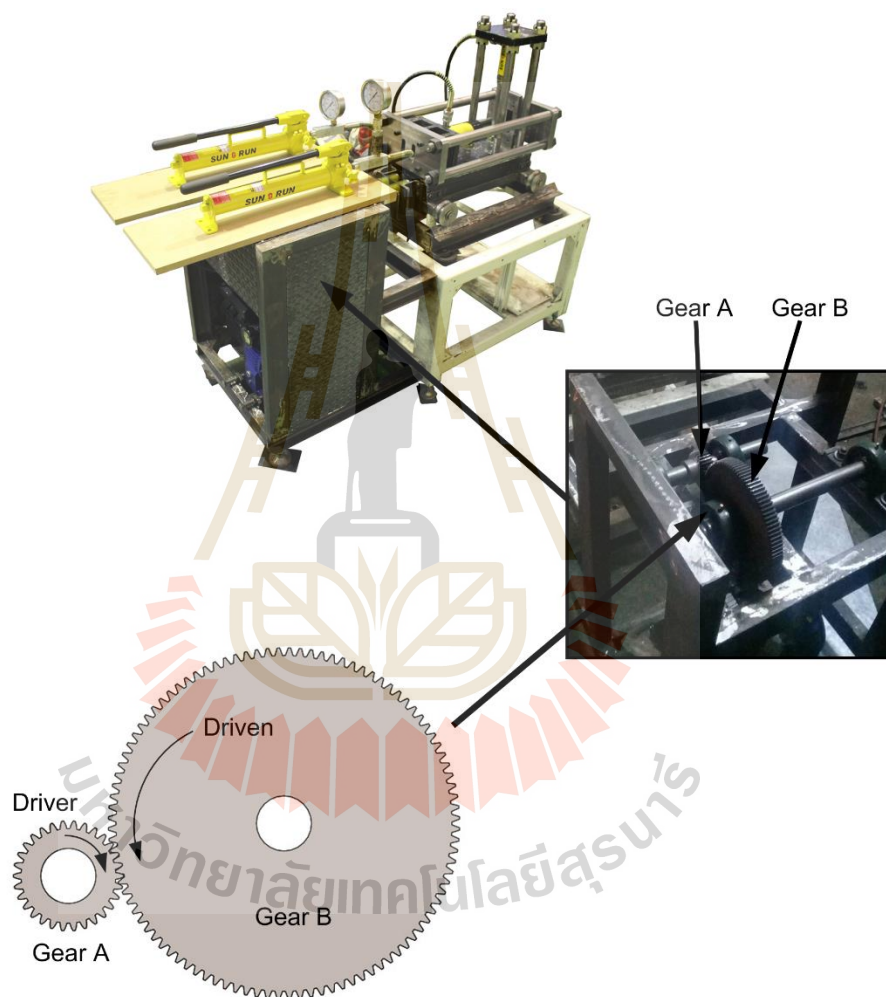
Figure 4.14 Spur gears are component of shaking table.

The shaking table was of the direct-drive type with a horizontal one-direction table motion. Results of calibration between horizontal acceleration and revolutions per minute (Figure 4.15). A check of the time-displacement characteristics of the table motion with the aid of the PiezoBEAM accelerometer (Figure 4.16). Table 4.4 shows the horizontal acceleration and revolutions per minute(rpm). The revolutions per minutes, period, frequency, acceleration, horizontal acceleration calculation from equation 4.1 and horizontal acceleration measured from PiezoBEAM accelerometer as shown in Table 4.5. The motion to be sinusoidal. Frequency were adjustable, the amplitude being from 8 centimeters and the frequency being variable from 64 to 135 cycles per minute or 1.067 to 2.25 Hz.
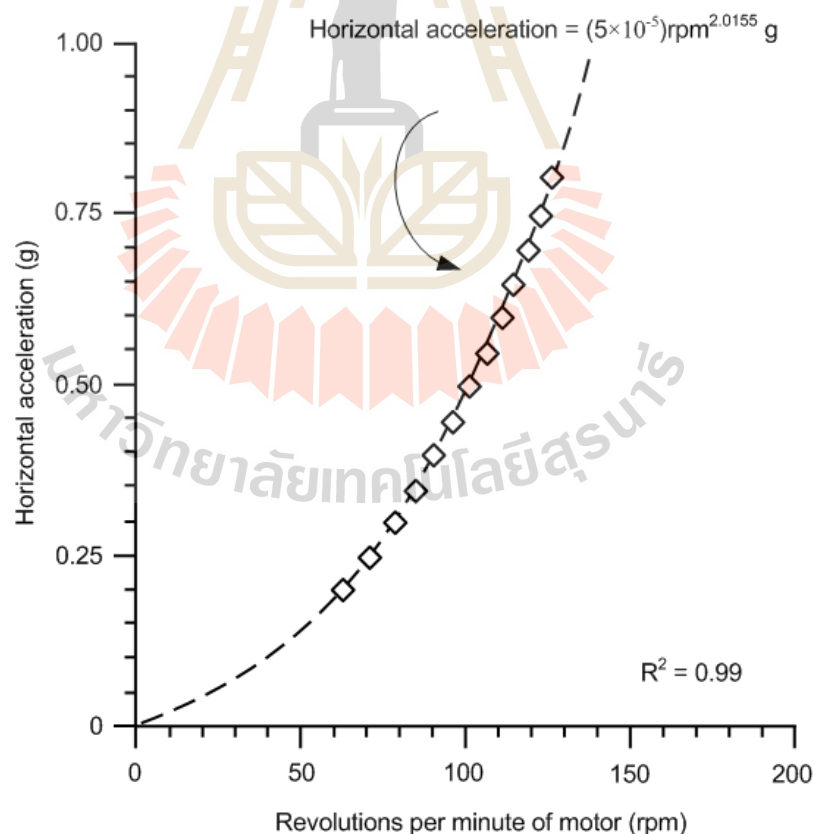
Figure 4.15   Results of calibration between horizontal acceleration and revolutions

per minute of a motor.

Table 4.4 Horizontal acceleration and revolutions per minute of a motor.

Revolutions per minute (rpm)	Horizontal acceleration (g)
64	0.20
72	0.25
79	0.30
85	0.35
91	0.40
96	0.45
101	0.50
106	0.55
111	0.60
115	0.65
120	0.70
124	0.75
128	0.80
132	0.85
135	0.90
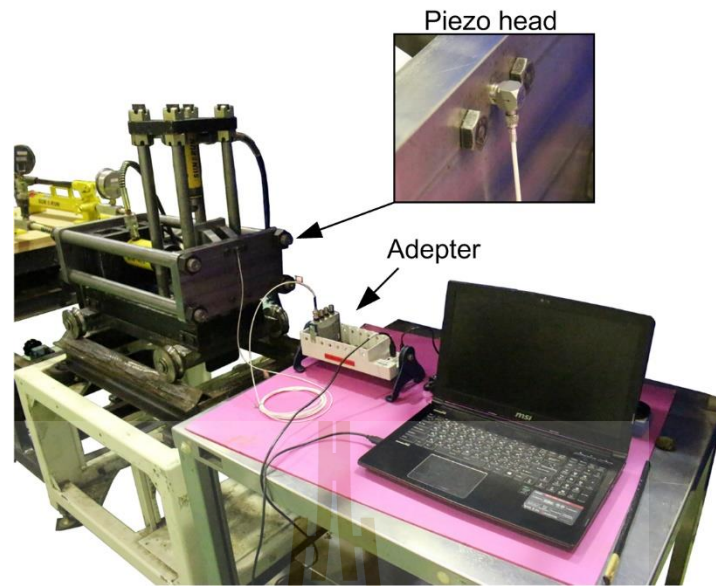
Figure 4.16 PiezoBEAM accelerometer

Table 4.5 Results of calibration between horizontal acceleration calculation from

equation 4.1 and PiezoBEAM accelerometer

RPM	Period (s)	Frequency (Hz)	Acceleration (m/s^2)	Horizontal acceleration from equation 4.1 (g)	Horizontal acceleration from PiezoBEAM (g)
64	0.937	1.07	1.977	0.200	0.20
72	0.833	1.20	2.503	0.250	0.25
79	0.759	1.31	3.013	0.307	0.30
85	0.706	1.41	3.488	0.350	0.35
91	0.659	1.51	3.998	0.407	0.40
96	0.625	1.60	4.450	0.450	0.45
101	0.594	1.68	4.926	0.500	0.50
106	0.566	1.76	5.425	0.550	0.55
111	0.540	1.85	5.949	0.600	0.60
115	0.521	1.91	6.386	0.650	0.65
120	0.500	2.00	6.953	0.708	0.70
124	0.484	2.06	7.425	0.750	0.75
128	0.468	2.13	7.911	0.806	0.80
132	0.454	2.20	8.414	0.857	0.85
135	0.444	2.25	8.800	0.890	0.90

CHAPTER V

LABORATORY TESTING

5.1   Introduction

The objective of the laboratory testing is to assess the effects of ground acceleration on fracture shear strengths by performing series of double fracture shear testing on Saw-cut and tension-induced fractures in Phra Wihan sandstone specimens.

5.2   Test method

The double-shear tests are performed with the normal stresses of 0.05 to 4 MPa for the smooth surfaces and the rough fractures. The test method and calculation follow as much as practical the ASTM (D5607-08) standard practice. Each specimen is sheared only once under the predefined constant normal stress using a direct shear machine (Double fracture shear device). Figure 5.1 shows the laboratory arrangement of the double shear test while the fracture is under normal and shear stresses. Three dial gages are used for monitoring the normal and shear displacement. The ground acceleration ranges are 0.0g, ,0.2, 0.3g, 0.4g, 0.5g, 0.6g, 0.7g and 0.8g. The shear force is continuously applied until a total shear displacement of 5 mm is reached. The applied normal and shear forces and the corresponding normal and shear displacements are monitored and recorded. Post-test observation on the sheared off area indicates that the asperity areas that have been sheared off are small for all specimens, about 10 - 20% of

the total areas. Figure 5.2 shows the pre and post-test fractures for the Phra Wihan

sandstone specimens.
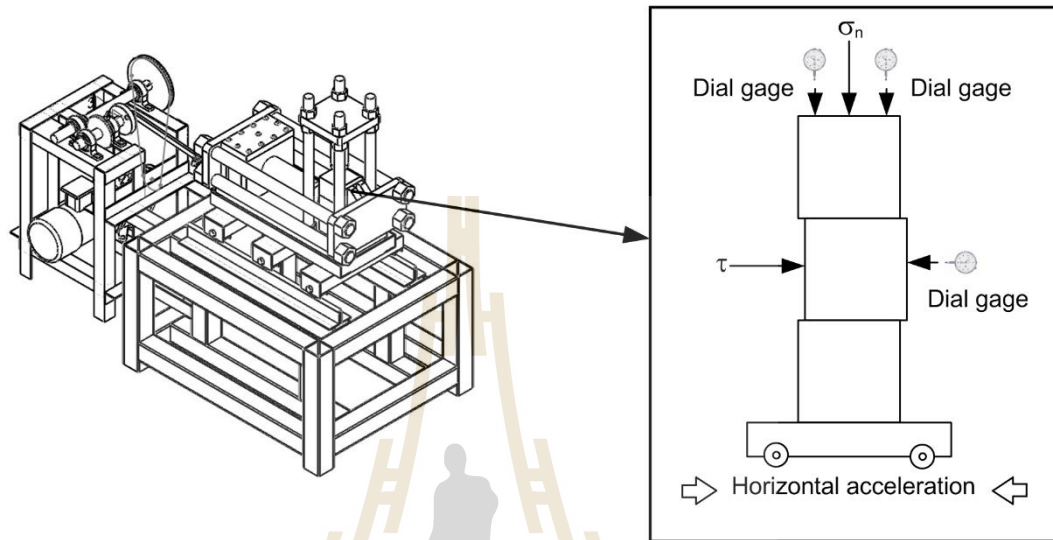
Figure 5.1 Test configurations

Figure 5.2 Pre-test and post-test Phra Wihan sandstone specimens.

5.3   Test Results

5.3.1 Saw-cut surfaces

The results are presented in terms of the shear stresses as a function of shear displacement under constant normal stresses from 0.05 to 4 MPa. Figures 5.3 through 5.7 show shear stresses of Phra Wihan sandstones as a function of shear displacement for various horizontal acceleration condition.   Figure 5.8 and 5.9 shows the shear strength of Phra Wihan sandstones as a function of normal stress for various horizontal acceleration (a_h). The shear strength are calculated by the equations (Hibbeler, 2011);

$$\tau = \frac{p}{A} \tag{5.1}$$

where P is the maximum shear force, and A is the contact area between both specimens (Double fracture areas is 2A). The shear strength of all specimens are summarized in Table 5.1 and shear parameter of all conditions are summarized in table 5.2.
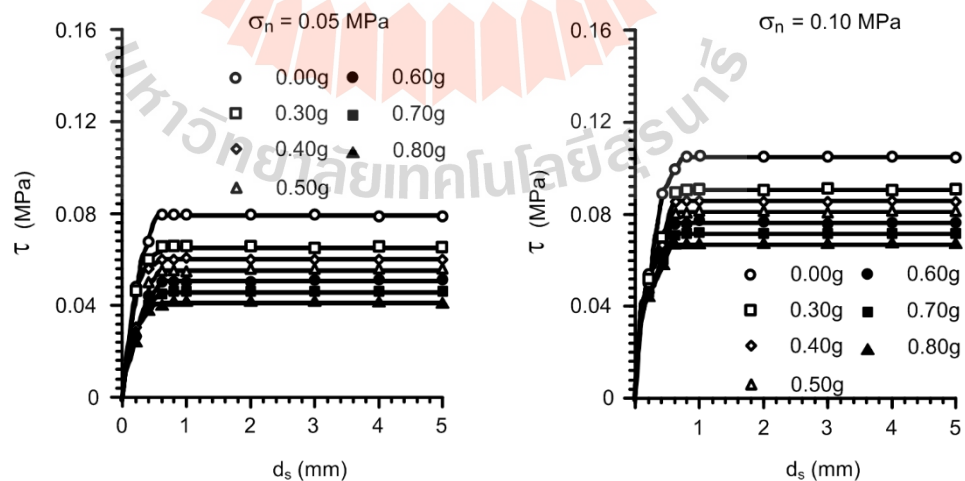
Figure 5.3   Shear stresses as a function of shear displacement under normal

stresses of 0.05 and 0.10 MPa.
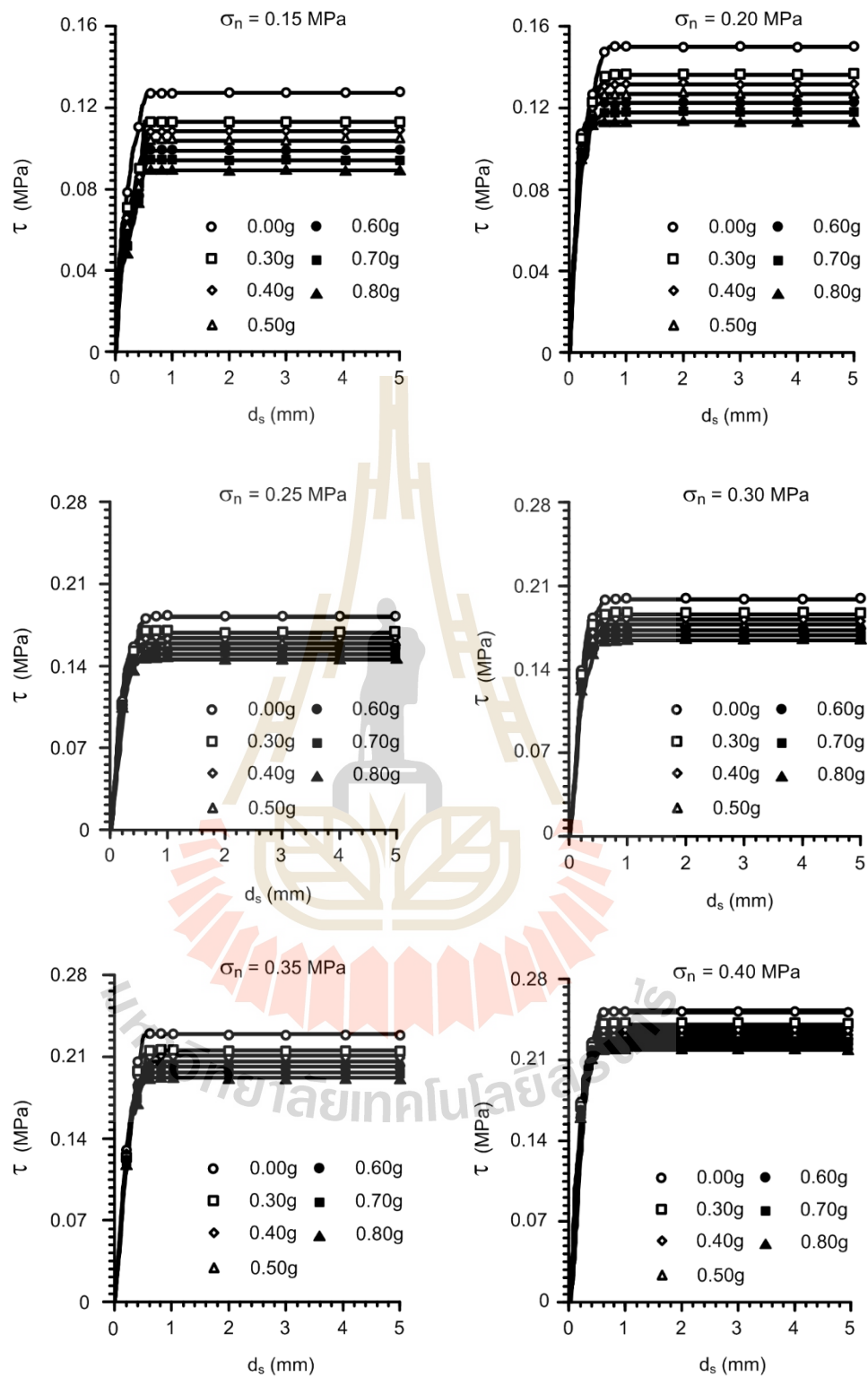
Figure 5.4   Shear stresses as a function of shear displacement under normal

stresses of 0.15, 0.20, 0.25, 0.30, 0.35 and 0.40 MPa.
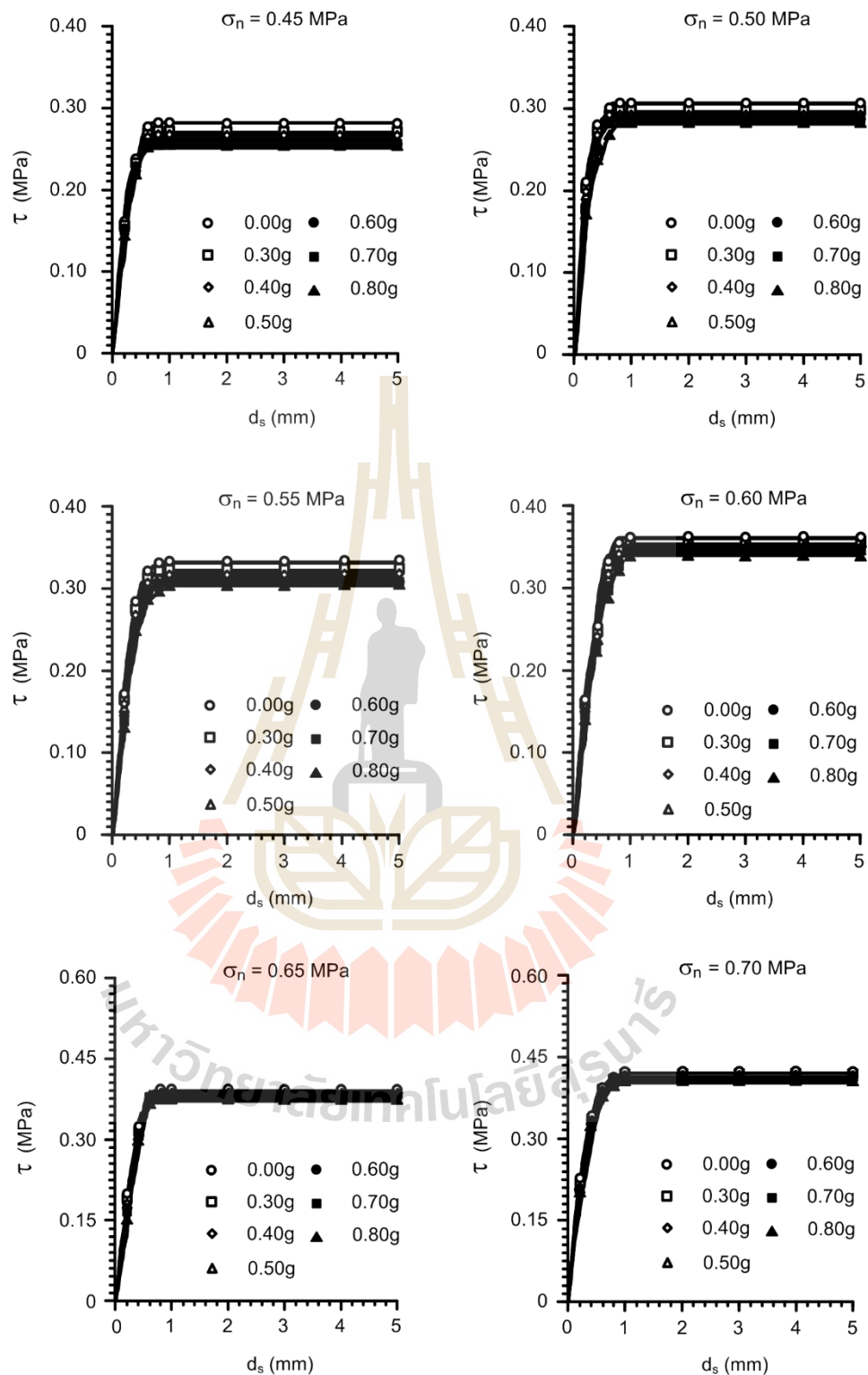
Figure 5.5   Shear stresses as a function of shear displacement under normal

stresses of 0.45, 0.50, 0.55, 0.60, 0.65 and 0.70 MPa.
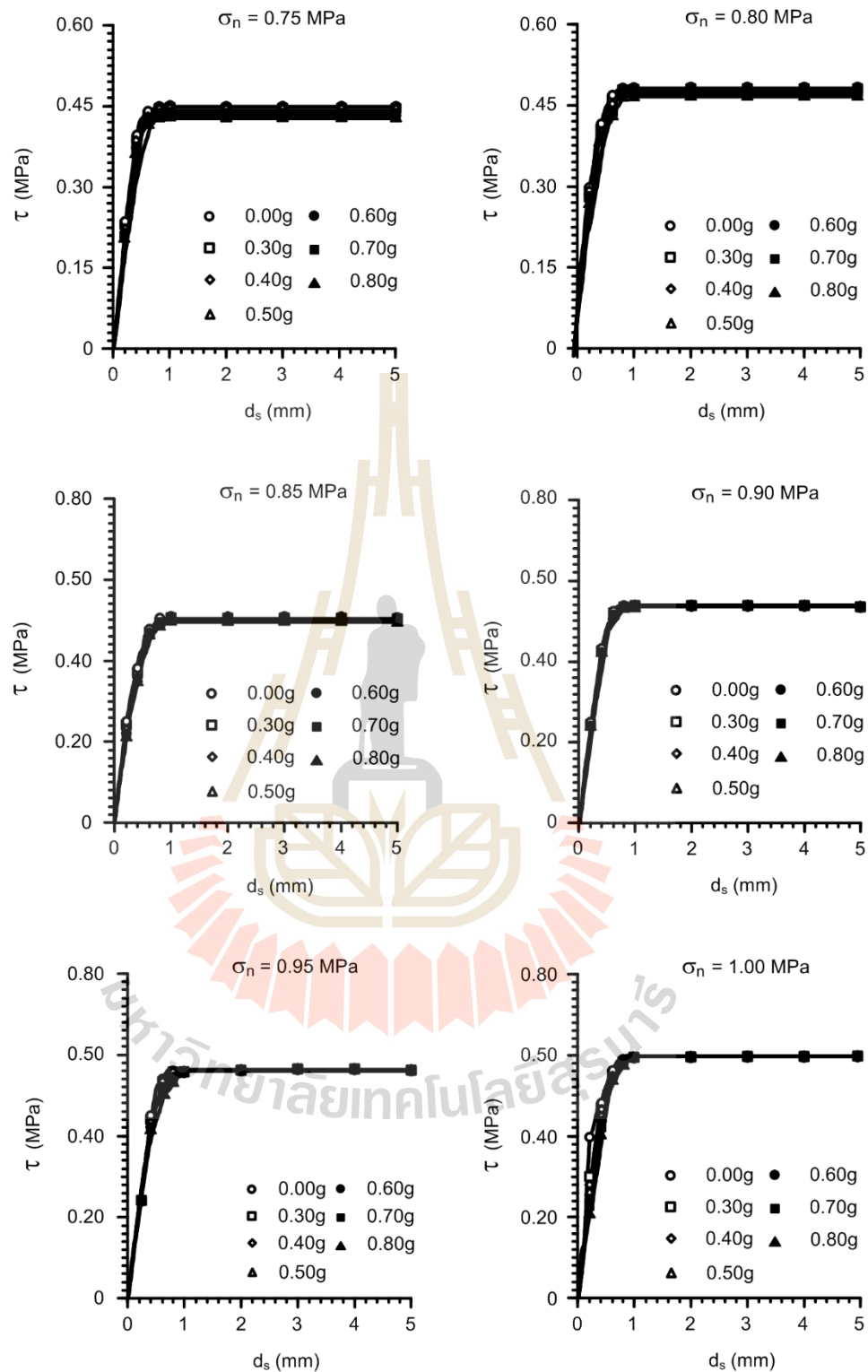
Figure 5.6   Shear stresses as a function of shear displacement under normal

stresses of 0.75, 0.80, 0.85, 0.90, 0.95 and 1.00 MPa.
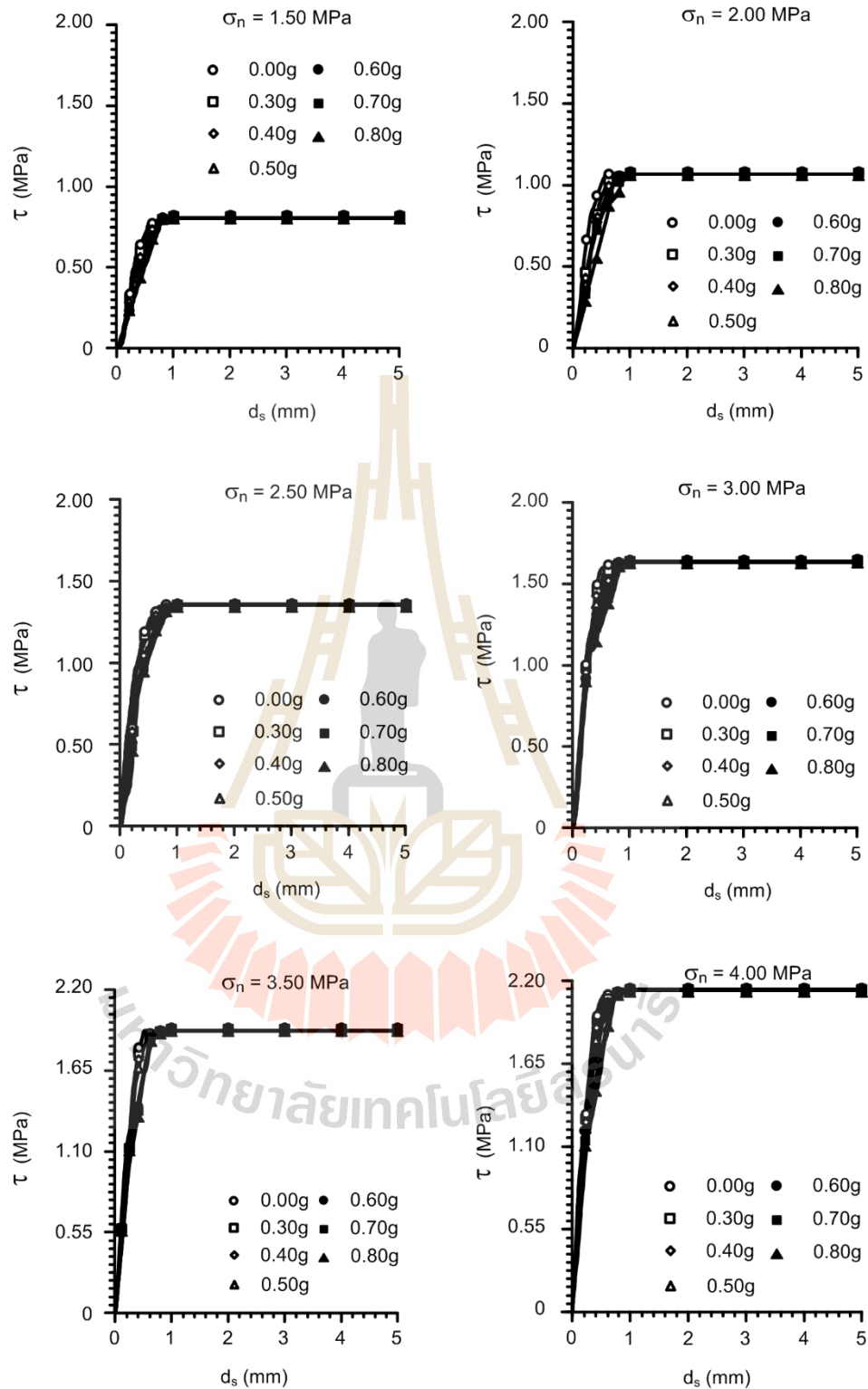
Figure 5.7   Shear stresses as a function of shear displacement under normal

stresses of 1.50, 2.00, 2.50, 3.00, 3.50 and 4.00 MPa.
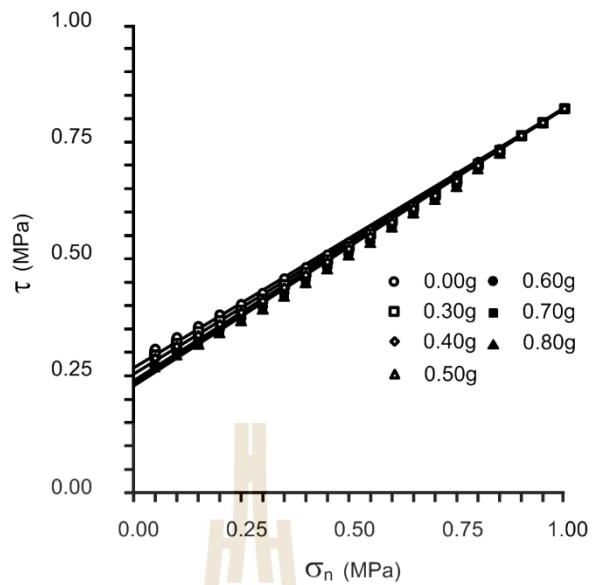
Figure 5.8   Shear strength of Phra Wihan sandstones as a function of normal

stress (0.05 to 1.00 MPa) for various horizontal acceleration.
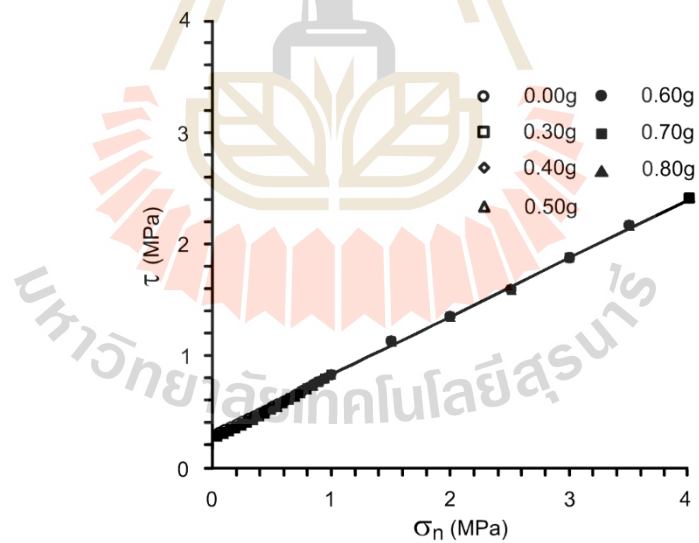
Figure 5.9   Shear strength of Phra Wihan sandstones as a function of normal

stresses (0.05 to 4.00 MPa) for various horizontal acceleration.

Table 5.1   Shear strength on saw-cut surfaces of all specimens are summarized.

Specimen No.	Density (g/cm^3)	Shear strength (MPa) Horizontal acceleration (g)							σ_n (MPa)
		0.0 g	0.3 g	0.4 g	0.5 g	0.6 g	0.7 g	0.8 g	
PW-01	2.28	0.080	0.065	0.061	0.056	0.051	0.046	0.042	0.05
		0.105	0.091	0.086	0.081	0.077	0.072	0.067	0.10
PW-02	2.29	0.129	0.114	0.109	0.105	0.100	0.095	0.090	0.15
		0.152	0.138	0.133	0.129	0.124	0.119	0.115	0.20
PW-03	2.31	0.176	0.163	0.158	0.154	0.149	0.145	0.140	0.25
		0.200	0.187	0.182	0.178	0.174	0.169	0.165	0.30
PW-04	2.29	0.231	0.217	0.212	0.207	0.202	0.197	0.193	0.35
		0.255	0.242	0.238	0.234	0.230	0.226	0.222	0.40
PW-05	2.29	0.282	0.270	0.266	0.262	0.258	0.255	0.251	0.45
		0.308	0.298	0.294	0.291	0.287	0.284	0.281	0.50
PW-06	2.25	0.335	0.325	0.321	0.318	0.314	0.311	0.307	0.55
		0.361	0.354	0.351	0.348	0.346	0.343	0.341	0.60
PW-07	2.26	0.391	0.383	0.380	0.378	0.375	0.373	0.371	0.65
		0.417	0.410	0.408	0.406	0.404	0.402	0.400	0.70
PW-08	2.34	0.452	0.441	0.439	0.436	0.433	0.431	0.428	0.75
		0.481	0.474	0.472	0.471	0.469	0.467	0.465	0.80
PW-09	2.32	0.507	0.504	0.503	0.502	0.501	0.500	0.499	0.85
		0.537	0.536	0.536	0.535	0.535	0.535	0.535	0.90
PW-10	2.43	0.565	0.564	0.564	0.563	0.563	0.563	0.563	0.95
		0.595	0.595	0.595	0.595	0.595	0.595	0.595	1.00
PW-11	2.38	0.835	0.835	0.835	0.835	0.835	0.835	0.835	1.50
		1.115	1.115	1.115	1.115	1.115	1.115	1.115	2.00
PW-12	2.32	1.380	1.380	1.380	1.380	1.380	1.380	1.380	2.50
		1.645	1.645	1.645	1.645	1.645	1.645	1.645	3.00
PW-13	2.32	1.902	1.902	1.902	1.902	1.902	1.902	1.902	3.50
		2.160	2.160	2.160	2.160	2.160	2.160	2.160	4.00

Table 5.2 Shear parameter on saw-cut surfaces of all conditions are summarized.

Horizontal acceleration (g)	Coulomb's criterion parameters		R^2
	Friction angle, ϕ (degrees)	Cohesion, c (MPa)	
0.0	28.54	0.042	0.99
0.3	29.20	0.025	0.99
0.4	29.46	0.019	0.99
0.5	29.72	0.013	0.99
0.6	29.94	0.007	0.99
0.7	30.16	0.001	0.99
0.8	30.41	0.000	0.99

5.3.2 Tension-induced fractures

The results are presented in terms of the shear stresses as a function of shear displacement under constant normal stresses at 0.05, 0.25, 0.50, 0.75, 1, 2, 3, and 4 MPa. Figures 5.10 through 5.11 show shear stresses of Phra Wihan sandstones as a function of shear displacement for various horizontal acceleration condition. Figure 5.12 show the shear strength as a function of normal stress for various horizontal acceleration (a_h). The shear strength are calculated by the equations 5.1. The shear strength of all specimens are summarized in Table 5.3 and shear parameter of all conditions are summarized in Table 5.4.

Figure 5.10 Shear stresses of tension-induced surfaces as a function of shear displacement under normal stresses of 0.05 and 0.25 MPa.

Figure 5.11 Shear stresses of tension-induced surfaces as a function of shear displacement under normal stresses of 0.50, 0.75, 1.00, 2.00, 3.00 and 4.00 MPa.
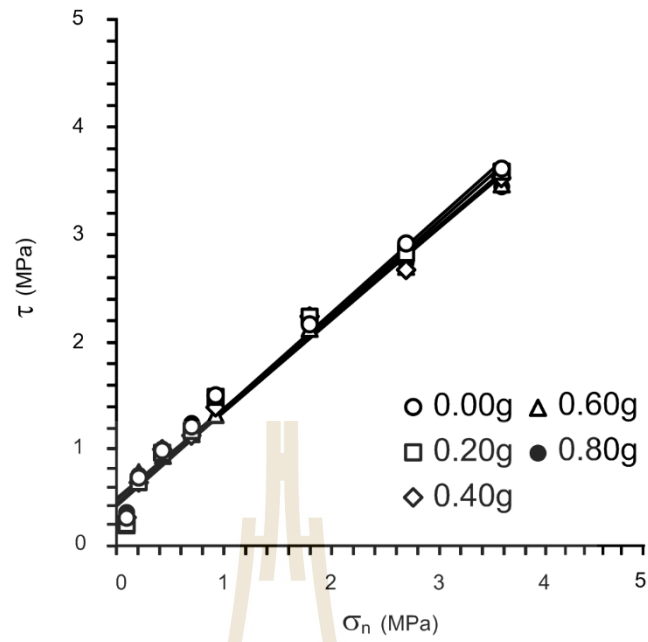
Figure 5.12   Shear strength of Phra Wihan sandstones as a function of normal
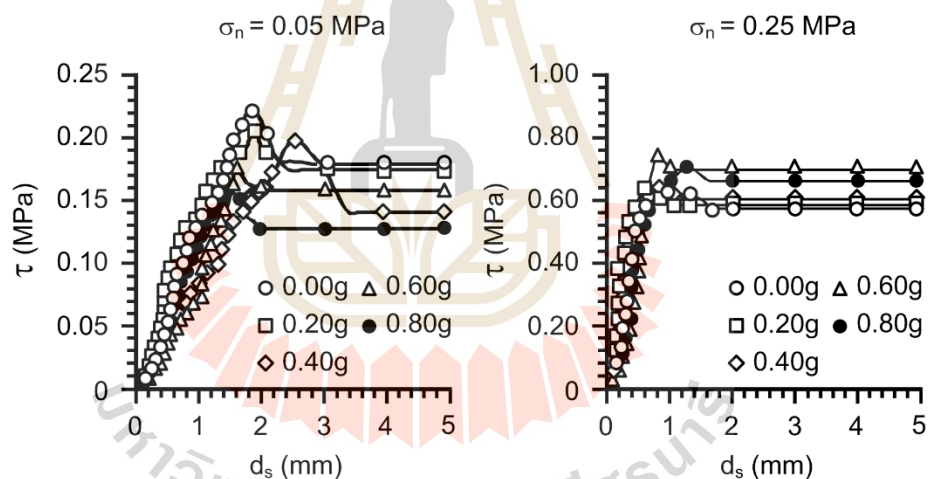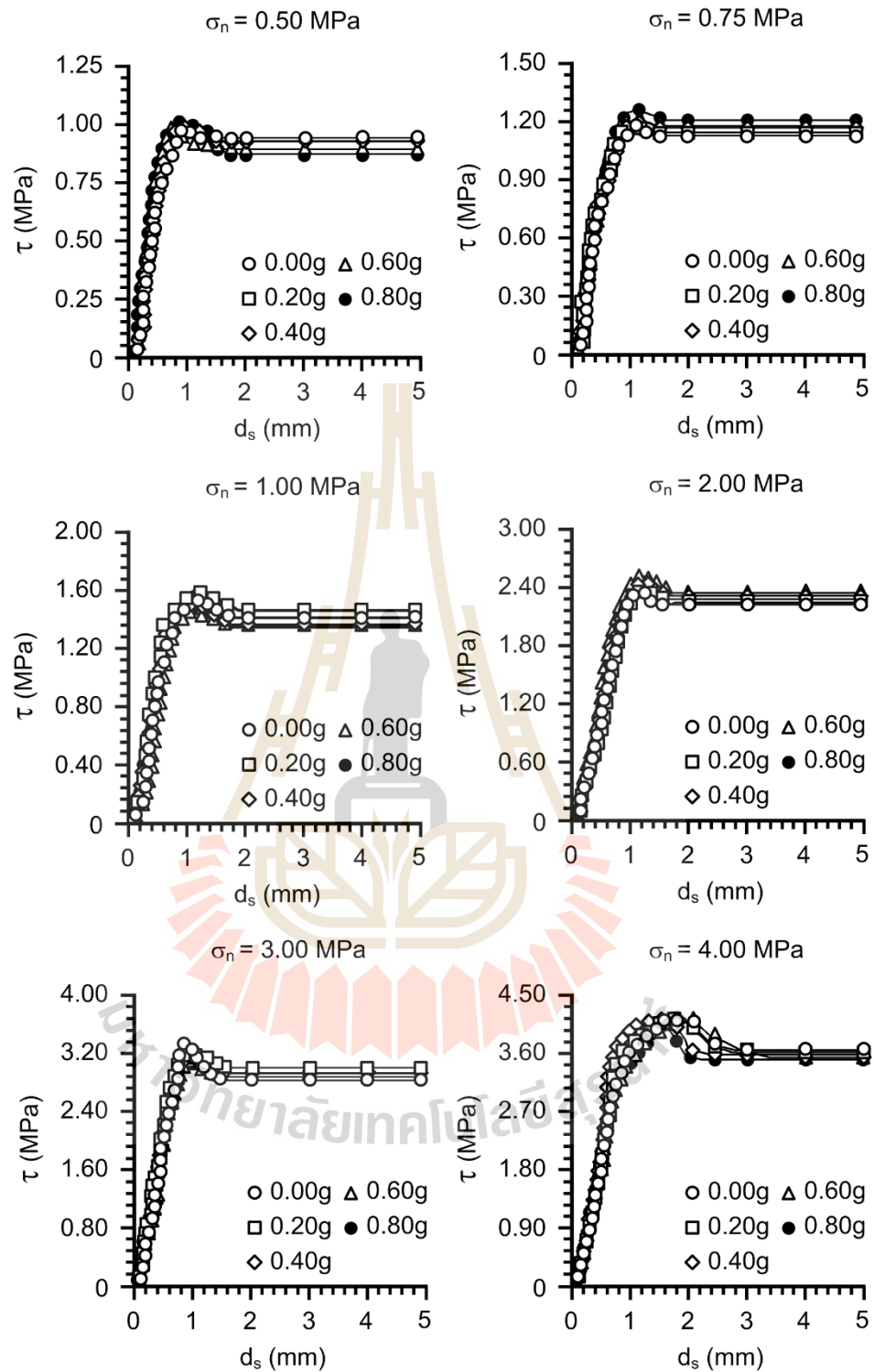
stresses 0.05, 0.25, 0.50, 0.75, 1.00, 2.00, 3.00, 4.00 MPa for various

horizontal acceleration.

Table 5.3 Shear strength on tension-induced fracture of all specimens are summarized.

Specimen No.	Density (g/cm^3)	JRC		Horizontal acceleration (g)	σ_n (MPa)	Shear strength (MPa)
		Top	Bottom			
PW-14	2.36	13	10	0.0g		0.198
PW-15	2.37	12	13	0.2g		0.144
PW-16	2.25	10	11	0.4g	0.05	0.211
PW-17	2.28	13	10	0.6g		0.156
PW-18	2.35	13	11	0.8g		0.224
PW-19	2.25	12	11	0.0g		0.645
PW-20	2.28	11	13	0.2g		0.649
PW-21	2.29	13	12	0.4g	0.25	0.645
PW-22	2.28	12	12	0.6g		0.742
PW-23	2.29	12	10	0.8g		0.706
PW-24	2.28	11	12	0.0g		0.998
PW-25	2.34	10	11	0.2g		0.961
PW-26	2.30	13	11	0.4g	0.50	1.005
PW-27	2.28	13	10	0.6g		0.966
PW-28	2.27	12	10	0.8g		0.984
PW-29	2.32	11	11	0.0g		1.177
PW-30	2.29	12	11	0.2g		1.195
PW-31	2.25	12	10	0.4g	0.75	1.236
PW-32	2.39	11	13	0.6g		1.229
PW-33	2.31	13	11	0.8g		1.283
PW-34	2.41	13	10	0.0g		1.605
PW-35	2.33	11	13	0.2g		1.577
PW-36	2.28	12	11	0.4g	1.00	1.506
PW-37	2.28	11	10	0.6g		1.442
PW-38	2.27	13	10	0.8g		1.502
PW-39	2.27	12	11	0.0g		2.416
PW-40	2.41	11	13	0.2g		2.482
PW-41	2.35	12	10	0.4g	2.00	2.497
PW-42	2.32	12	11	0.6g		2.420
PW-43	2.32	11	12	0.8g		2.467

Table 5.3 Shear strength on tension-induced fracture of all specimens are summarized (continued).

Specimen No.	Density (g/cm³)	JRC		Horizontal acceleration (g)	σ_n (MPa)	Shear strength (MPa)
		Top	Bottom			
PW-44	2.36	12	13	0.0g		3.306
PW-45	2.37	11	12	0.2g		3.192
PW-46	2.25	13	12	0.4g	3.00	3.061
PW-47	2.28	11	12	0.6g		3.116
PW-48	2.35	13	11	0.8g		3.153
PW-49	2.25	12	11	0.0g		4.166
PW-50	2.28	13	11	0.2g		4.124
PW-51	2.29	12	12	0.4g	4.00	4.083
PW-52	2.28	13	11	0.6g		4.041
PW-53	2.29	11	12	0.8g		3.999

Table 5.4 Shear parameter on tension-induced fracture of all conditions are summarized.

Horizontal acceleration (g)	Coulomb's criterion parameters		R^2
	Friction angle, ϕ (degrees)	Cohesion, c (MPa)	
0.0	43.80	0.42	0.98
0.2	43.50	0.42	0.98
0.4	42.53	0.45	0.98
0.6	42.50	0.44	0.98
0.8	42.17	0.48	0.98

CHAPTER VI

MATHEMATIC RELATIONS

6.1   Introduction

The objective of this chapter is to develop mathematic equations to describe the effects of ground acceleration with saw-cut and tension-induced fractures.   The Coulomb criterion is applied to the results.

6.2   Coulomb Criterion

Based on the Coulomb criterion, the shear stress (τ) can be represented by:

$$\tau = c + \sigma_n \tan\phi \tag{6.1}$$

where σ_n is the normal stress, c is the cohesion and ϕ is the friction angle.

6.2.1   Saw-cut fractures

The friction angle (ϕ) and cohesions (c) under horizontal acceleration test conditions are shown in Table 6.1.   They can be determined as a function of the horizontal acceleration with saw-cut fractures as follows (Figure 6.1):

$$\delta = \alpha G + \beta \tag{6.2}$$

$$\xi = \gamma G + \eta \tag{6.3}$$

where δ and ξ are defined here as the apparent friction angle and apparent cohesion of the fractures on horizontal acceleration condition, G is the horizontal acceleration (g), α, β, γ, η are empirical as show in table 6.2. Substituting equations (6.2) and (6.3) into (6.1), the shear strength (τ) can be written as:

$$\tau = (\alpha G + \beta)\sigma_n +(\gamma G + \eta) \tag{6.4}$$

Figure 6.2 shows the compared shear strength under various horizontal ground acceleration based on Coulomb derived equation and result tested. The result is fit similar.

Table 6.1 Friction angle (ϕ) and cohesions (c) under saw-cut fracture with

horizontal ground acceleration test conditions.

Horizontal acceleration (g.)	Friction angle (angle)	Cohesion (MPa)	R^2
0	28.661	0.265	0.99
0.3	29.244	0.248	0.99
0.4	29.479	0.242	0.99
0.5	29.713	0.237	0.99
0.6	29.946	0.231	0.99
0.7	30.178	0.225	0.99
0.8	30.408	0.219	0.99
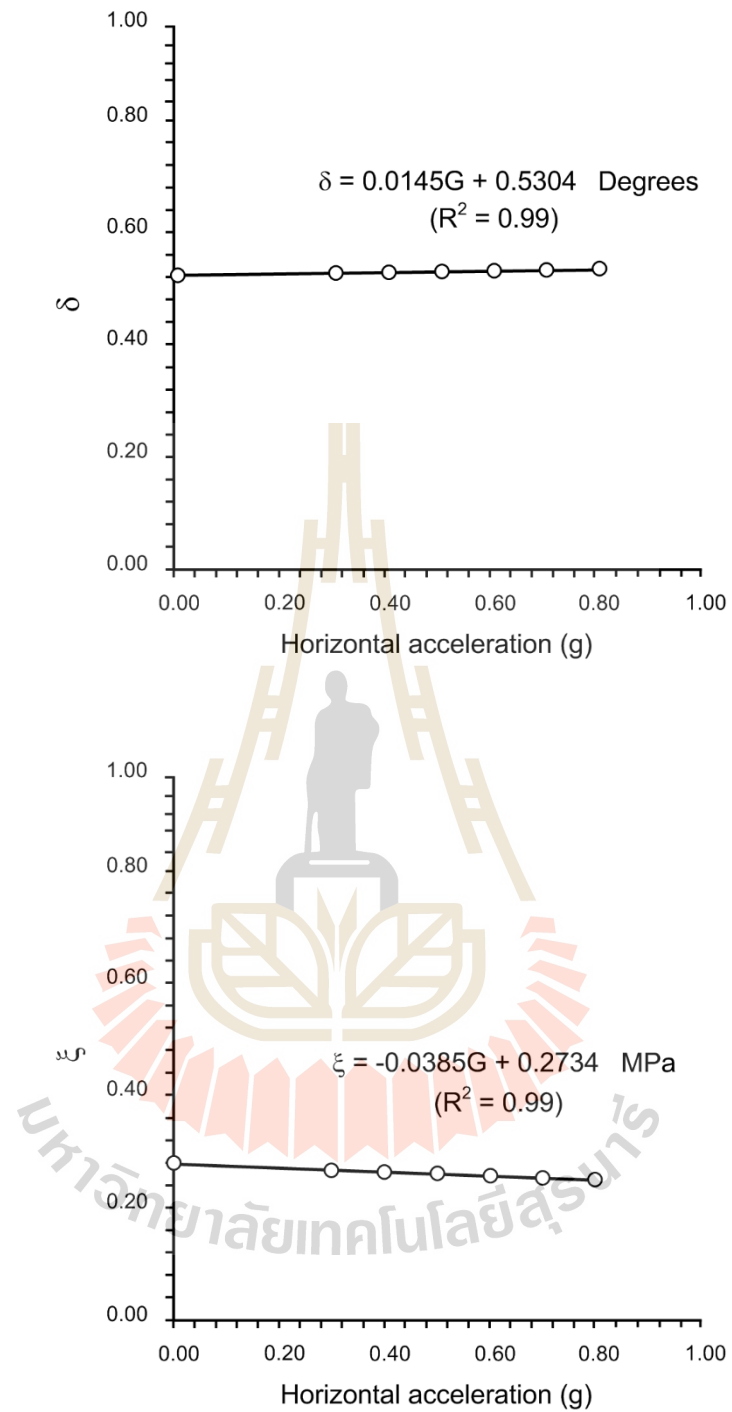
Figure 6.1 Cohesion (ξ) and friction angle (δ) as a function of the ground

acceleration (g) with saw-cut fractures.

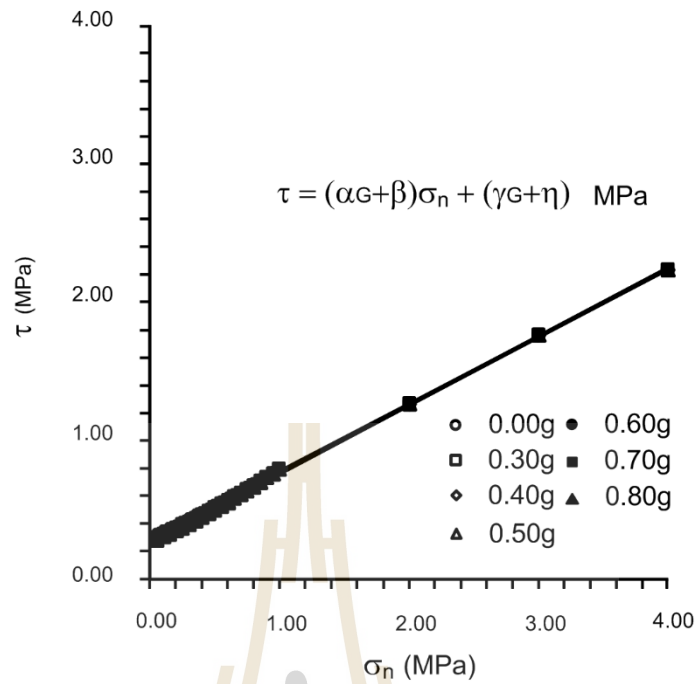**Figure 6.2** Comparison of the shear strength of saw-cut fractures based on

Coulomb derived equation (line) and result tested (symbol).

Table 6.2 Empirical constants of shear strength of saw-cut fracture.

Empirical Constant	value
α	0.0145
β	0.5304
γ	-0.0385
η	0.2734

6.2.2 Tension-induced fractures

Figure 6.3 shows the compared shear strength on tension-induced fractures under various horizontal ground acceleration based on Coulomb equation and result tested, τ as a function of the normal stress. The friction angle (ϕ) and cohesions (c) under horizontal acceleration test conditions are shown in Table 6.3. The shear strength tends to linearly increase with increasing the normal stress which can be represented by:

$$\tau = \delta_R \sigma_n + \xi_R \tag{6.5}$$

where δ_R and ξ_R are defined here as the apparent friction angle and apparent cohesion of the tension-induced fractures on horizontal acceleration condition.

$$\delta_R = \alpha_R G + \beta_R \tag{6.6}$$

$$\xi_R = \gamma_R G + \eta_R \tag{6.7}$$

where G is the horizontal acceleration (g.), α_R, β_R, γ_R and η_R are empirical as show in table 6.4. Substituting equations (6.6) and (6.7) into (6.1), the shear strength (τ) can be written as:

$$\tau = (\alpha_R G + \beta_R)\sigma_n + (\gamma_R G + \eta_R) \tag{6.8}$$

They can be determined as a function of the horizontal acceleration with tension-induced fractures as follows (Figure 6.4):

Table 6.3 Friction angle (φ) and cohesions (c) under tension-induced fractures with

horizontal acceleration test conditions.

Horizontal acceleration (g.)	Friction angle (degree)	Cohesion (MPa)	R^2
0.0	43.801	0.429	0.98
0.2	43.504	0.421	0.98
0.4	42.583	0.454	098
0.6	42.505	0.441	0.98
0.8	42.167	0.482	0.98
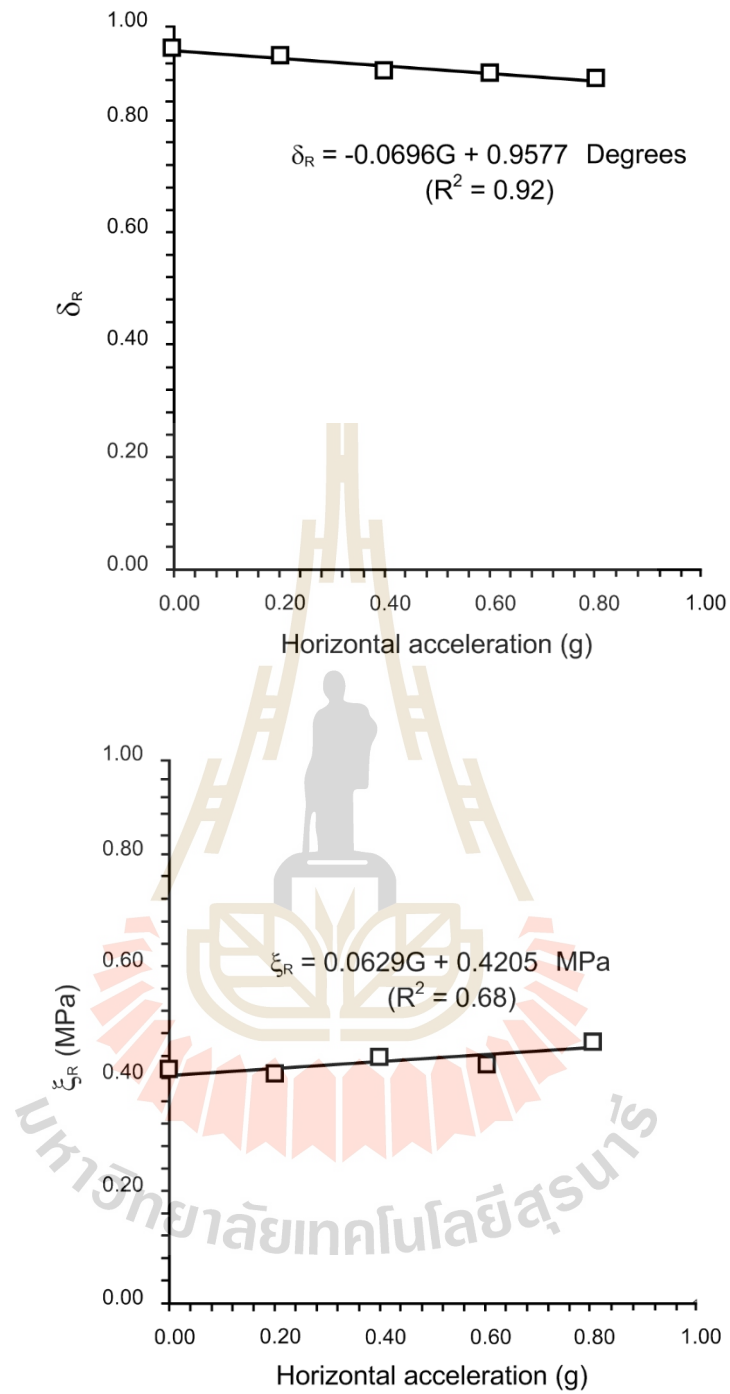
Figure 6.3 Cohesion (ξ_R) and friction angle (δ_R) as a function of the horizontal

acceleration (g) with tension-induced fractures.

$$\tau = (\alpha_R G + \beta_R)\sigma_n + (\gamma_R G + \eta_G) \text{ MPa}$$

Figure 6.4 Comparison of the shear strength of tension-induced fractures under

horizontal acceleration base on coulomb derived equation (line) and result

tested (symbol).

Table 6.4 Empirical constants of shear strength of tension-induced fracture.

Empirical constant	value
α_R	-0.0696
β_R	0.9577
γ_R	0.0629
η_R	0.4205

CHAPTER VII

DISCUSSIONS, CONCLUSIONS, AND RECOMMENDATIONS FOR

FUTURE STUDIES

8.1 Discussions

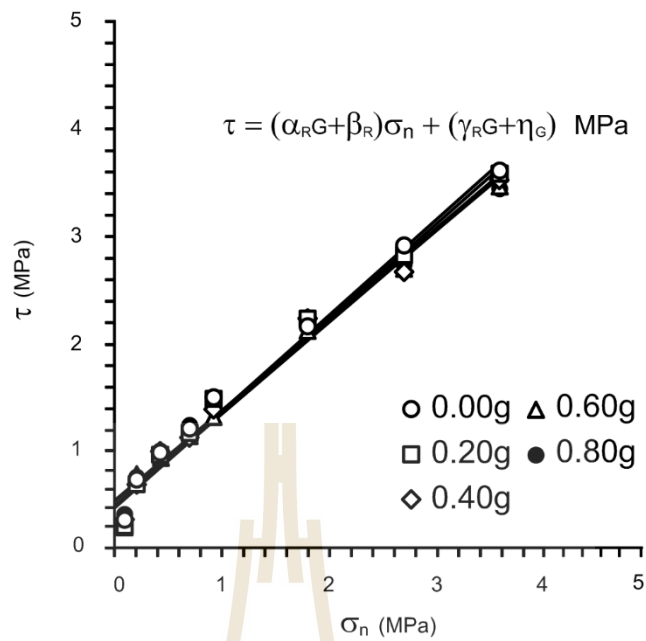Double fracture shear test is performed under constant normal load (CNL) condition which the normal load is maintained constant during the shearing process. The testing is conducted under static and dynamic conditions on smooth and rough surface specimens of Phra Wihan sandstone. Dynamic condition used in this study has an earthquake acceleration of 0.2g to 0.8g, which is a one-dimensional acceleration. The results indicate that the shear strengths on smooth surface increase with increasing normal stresses and decrease with increasing horizontal acceleration, whereas the shear strength on rough surface slightly fluctuates. The results clearly show that the earthquake vibration in one-dimensional very slightly affect to the shear strength for all testing, especially under high normal loads.

The mathematical equations based on Coulomb criteria that explicitly incorporate the effects of horizontal acceleration is proposed to estimate the shear strengths. The empirical equations fit well to the test results for both saw-cut and tension-induced fractures.

8.2 Conclusions

The results show that the shear strength on smooth surface tends to decrease when the normal stresses approach zero, whereas the shear strength on rough surfaces slight fluctuates. The friction angle of saw-cut fractures is 29.64±0.63° and of tension-induced fractures is 42. 91±0. 70°. The results clearly show that the earthquake

acceleration in one-dimensional very slightly affect to the shear strength for all testing, especially under high normal loads. This is because the double-shear test is performed under constant normal load throughout the shearing which is agrees with the results obtained by Sakulnitichai et al. (2009) and Kleepmeak et al. (2013) who investigate the effects of earthquake acceleration one-dimensional on the stability of rock which is under unconfinement condition. Sakulnitichai et al. (2009) suggest that the dynamic load more affect the stability of shallow underground excavation (low confinement) in jointed rock mass than in deep underground excavation, and the impact of the dynamic loads also reduces as the depth increases (high confinement). Hack et al. (2007) suggest that during the earthquake, the horizontal acceleration adds an unfavorably oriented force to the blocks that may cause instability. The acceleration also reduces normal stresses on the contact plane. The findings can be used for the analysis and design of engineering structures in fractured rock mass under earthquake conditions and blasting activities.

8.3 Recommendations for future studies

The study in this research can be taken as a preliminary guideline and process of study and design. More rock types should be tested under various ranges of ground acceleration. The shearing rates should be applied at wider ranges of normal stress and rates, or other forms of testing, such as testing under saturated condition of rock specimen to simulate for rock structure near the wetlands.

REFERENCES

ASTM D 5607-08. Test method for performing laboratory direct shear strength tests of rock specimens under constant normal force. **Annual Book of ASTM Standards.** 04.08. West Conshohocken: American Society for Testing and Materials: Philadelphia.

Baraza, J., Ercilla, G. and Lee, J. (1992). Geotechnical properties and preliminary assessment of sediment stability on the continental slope of the Northwestern Alboran Sea. **Geo-Marine Letters.** 12: 150-156.

Barton, N. and Hansteen, H. (1979). Very large span openings at shallow depth: deformation magnitudes from jointed models and finite element analysis. In **Proceedings of the 4th Excavation and Tunnelling Conference.** 2: 1331-1353. Atlanta.

Barton, N. R. (1973). Review of a new shear strength criterion for rock joints. **Engineering Geology.** 7: 287-332.

Chen, T. C., Lin, M. L., and Hung, J. J. (2003). Pseudostatic analysis of Tsaoling rockslide caused by Chi-Chi Earthquake. **Engineering Geology.** 71(1): 31-47.

Crawford, A. M., and Curran, J. H. (1981, December). The influence of shear velocity on the frictional resistance of rock discontinuities. **International Journal of Rock Mechanics and Mining Sciences and Geomechanics Abstracts.** 18(6): 505-515). Pergamon.

CDMG (1997) Guidelines for Evaluating and Mitigating Seismic Hazards in California. **California Div. of Mines and Geology, Special Publication.** 117: www/consrv.ca.gov/dmg/pubs/sp/117/

Daisuke, M., Hiroshi, C., Kaoru, K. and Kazunobu, M. (2003). Underground large cavern with shallow overburden considered earthquake protection against disasters. **In Proceedings of the Symposium on Underground Space.** 8: pp 267-272. Japan.

Dowding, C.H., and Rozen, A 1978. Damage to rock tunnels for earthquake shaking Journal of the Geotechnical Engineering Division, **American Society of Civil Engineers.** p. 104 GT2

Gendzwill, D. (2008). **Glossary of Seismic Techniques and Terminology.** [Online]. Available: http://www.usask.ca/geology/labs/seismo/glossary.html

Genis, M. and Aydan, O. (2002). Evaluation of dynamic response and stability of shallow underground openings in discontinuous rock masses using model tests. **Proceeding. of 2002 ISRM Regional Symposium (3rd Korea-Japan Joint Symposium) on Rock Engineering Problems and Approaches in Underground Construction** (Vol. 2, pp 787-794.). Seoul.

Ghosh, A., Hsiung, S.M., and Chowdhury, A.H. 1996 Seismic Response of Rock Joints and Jointed Rock Mass. **Division of Regulatory Applications Office of Nuclear Regulatory Research U.S. Nuclear Regulatory Commission Washington, DC.** 20555-0001 NRC FIN B6643

Hack, R., Alkema, D., Kruse, G.A.M., Leenders, N., and Luzi, L. (2007). Influence of earthquakes on the stability of slopes. **Engineering Geology**. 91:4-15.

Hashash, Y.M.A., Hook, J.J., Schmidt, B., and Yao, J.I.C. 2001 seismic design and analysis of underground structures. **Tunneling and Underground Space Technology.** 16: pp. 247-293.

Hencher, S. R., and Richards, L. R. (1989). Laboratory direct shear testing of rock discontinuities. **Ground Engineering.** 22(2): 24-31.

Hibbeler, R.C. 2011. **Mechanics of Materials.** Person Prentice Hall, United States of America, 32 pp.

Hosseini, K. A., Pellet, F., Jafari, M. K., and Boulon, M. (2004). Shear strength reduction of rock joints due to cyclic loading. **Proceedings of the 13th World Conference on Earthquake Engineering** (Paper No. 3070). Vancouver, B.C., Canada, 8 pp.

Itasca (1994). **User Manual for FLAC-Fast Langrangian Analysis of Continua,** Version 4.0. Itasca Consulting Group Inc. Minneapolis, Minnesota.

Jafari, M. K., Hosseini, K. A., Pellet, F., Boulon, M., and Buzzi, O. (2003). Evaluation of shear strength of rock joints subjected to cyclic loading. **Soil Dynamics and Earthquake Engineering.** 23(7): 619-630.

Jafari, M. K., Shafiee, A., and Razmkhah, A. (2002). Dynamic properties of fine grained soils in south of Tehran. **Journal of Seismology and Earthquake Engineering.** 4(1): 25.

Kamonphet, T., Khamrat, S., and Fuenkajorn, K. (2015). Effects of cyclic shear loads on strength, stiffness and dilation of rock fractures. **Songklanakarin Journal of Science and Technology,** 37(6).

Kemthong, R. and Fuenkajorn, K. (2007). Prediction of joint shear strengths of ten rock types using field-identified parameters. **Proceedings of the First Thailand Symposium on Rock Mechanics, Khao Yai,** Thailand, Geomechanics Research Unit, Institute of Engineering Suranaree University of Technology, Thailand pp.195-209.

Kramer, S. L. (1996). Geotechnical earthquake engineering. New Jersey: Prentice Hall. Lama, R.D. and Vutukuri, V.S. (1978). **Handbook on Mechanical Properties of Rocks.** Vol. 4. Trans Tech Publication.

Kwafniewskil, M.A. and Wang, J.A. (1997). Surface roughness evolution and mechanical behavior of rock joints under shear. **International Journal of Rock Mechanics and Mining Sciences.** 34 (3-4): 157.e1-157.e14.

Lee, H.S., Park, Y.J., Cho, T.F. and You, K.H. (2001). Influence of asperity degradation on the mechanical behavior of rough rock joints under cyclic shear loading. **International Journal of Rock Mechanics and Mining Sciences.** 38(7): 967-980.

Lenhardt, W. A. (2009). The impact of earthquakes on mining operations. BHM Bergund Hüttenmännische Monatshefte, 154(6): 249-254.

Liu, X. G., Zhu, W. C., Yu, Q. L., Chen, S. J., and Li, R. F. (2017). Estimation of the joint roughness coefficient of rock joints by consideration of two-order asperity and its application in double-joint shear tests. **Engineering Geology.** 220: 243-255.

Kleepmek, M., and Fuenkajorn, K. (2013). Laboratory simulations of effects of joint spacing and joint angle on rock slope stability. In: **Rock Mechanics Proceedings of the Fourth Thailand Symposium, Im Poo Hill Resort, Nakhon Ratchasima.**

Nguyen, V. H. (2013). Static and Dynamic Behaviour of Joints in Schistose Rock: Lab Testing and Numerical simulation. **Ph.D. thesis.** Faculty of Geosciences, Geoengineering and Mining of the Technische Universität Bergakademie Freiberg, Germany.

Owen, G. N. and Scholl, R. E. (1981). Earthquake Engineering of Large Underground Structures. **San Francisco; URS/Blume (John A.) and Associates.**

Pangpetch, P. and Fuenkajorn, K. (2007). Simulation of rock slope failure using physical model. **Proceedings of the First Thailand Symposium on Rock Mechanics. Suranaree University of Technology** (pp 227-243). Nakhon Ratchasima.

Park, J.W. and Song, J.J. (2009). Numerical simulation of a direct shear test on a rock joint using a bonded-particle model. **International Journal of Rock Mechanics and Mining Sciences.** 46(8): 1315-1328.pp 165-187.

Prasad, S. K., Towhata, I., Chandradhara, G. P., and Nanjundaswamy, P. (2004). Shaking table tests in earthquake geotechnical engineering. **Current science Bangalore.** Mysore, India. 87: 1398-1404.

Richter, C. (1958). **Elementary Seismology.** W.H. Freeman and Co., San Francisco, and Bailey Bros. & Swinfen Ltd., London.

Sakulnitichai, C., Pangpetch, P., and Fuenkajorn, k. (2009). Physical model simulation of shallow openings in jointed rock mass under static and dynamic loads. In **Proceeding of the Second Thailand Symposium on Rock Mechanics** (pp. 147-160). Chonburi: Thailand.

Seismological Bureau, (2014). **Earthquake Report in Thailand and Adjacent countries.** Meteorological department. 90p.

Silva, P.G., Goy, J.L., Zazo, C., Bardaji, T., Lario, J., Somoza, L., Luque, L., and Gonzalez-Hernandez, F.M. (2006). Neotectonic fault mapping at the Gibraltar Strait Tunnel area, Bolonia Bay (South Spain). **Engineering Geology** 84(1): 31-47.

Terzaghi, K. 1950. **Mechanism of Landslides.** Geological Society of America, Berkeley. pp. 83-125.

Wald, D. A., Quitoriano, V., Heaton, T. H. and Kanamori, H. (1999). Relationships between peak ground acceleration, peak ground velocity, and modified Mercalli intensity in California. **Earthquake Spectra.** 15: 557-564.

Woodward, P. K., and Griffiths, D. V. (1996). Comparison of the pseudo-static and dynamic behaviour of gravity retaining walls. **Geotechnical and Geological Engineering.** 14(4): 269-290.

Zhang, Y., Wang, J., Xu, Q., Chen, G., Zhao, J. X., Zheng, L., and Yu, P. (2015). DDA validation of the mobility of earthquake-induced landslides. **Engineering Geology.** 194: 38-51.

BIOGRAPHY

Mister khanaphot boonyord was born on February 3, 1992 in Burirum, Thailand. He received her Bachelor's Degree in Engineering (Geotechnology) from Suranaree University of Technology in 2015. For her post-graduate, she continued to study with a Master's degree in the Geological Engineering Program, Institute of Engineering, Suranaree university of Technology. During graduation, 2016-2018, He was a part time worker in position of research assistant at the Geomechanics Research Unit, Institute of Engineering, Suranaree University of Technology.